PROF. WEIXING SHAN (Orcid ID : 0000-0001-7286-4041)

Article type : Regular Manuscript

Negative regulators of plant immunity derived from cinnamyl alcohol dehydrogenases are targeted by multiple *Phytophthora* Avr3a-like effectors

Tingting Li[1], Qinhu Wang[1], Ruirui Feng[1], Licai Li[1], Liwen Ding[1], Guangjin Fan[1], Weiwei Li[1], Yu Du[1], Meixiang Zhang[1], Guiyan Huang[1], Patrick Schäfer[2, 3], Yuling Meng[1], Brett M. Tyler[4], Weixing Shan[1,*]

[1] State Key Laboratory of Crop Stress Biology for Arid Areas and College of Agronomy, Northwest A&F University, Yangling, Shaanxi 712100, China.

[2] School of Life Sciences, University of Warwick, Gibbet Hill Campus, Coventry, CV4 7AL, UK

[3] Warwick Integrative Synthetic Biology Centre, University of Warwick, Coventry, CV4 7AL, UK

[4] Center for Genome Research and Biocomputing and Department of Botany and Plant Pathology, Oregon State University, Corvallis, OR 97331, USA

* Correspondence: Weixing Shan (Tel: +86-029-8708 0102, E-mail: wxshan@nwafu.edu.cn)

Received: 5 June 2019

Accepted: 15 August 2019

ORCIDs: Tingting Li: 0000-0002-5011-0174; Qinhu Wang: 0000-0003-1251-073X; Patrick Schäfer: 0000-0002-0366-6858; Brett M. Tyler: 0000-0003-1549-2987; Weixing Shan: 0000-0001-7286-4041

Summary

- Oomycete pathogens secrete numerous effectors to manipulate host immunity. While some effectors share a conserved structural fold, it remains unclear if any have conserved host targets. Avr3a-like family effectors, which are related to *Phytophthora infestans* effector PiAvr3a and widely distributed across diverse clades of *Phytophthora* species, were employed to study this question.
- By using yeast-two-hybrid, bimolecular fluorescence complementation, and co-immunoprecipitation assays, we identified members of the plant cinnamyl alcohol dehydrogenase 7 (CAD7) subfamily as targets of multiple Avr3a-like effectors from *Phytophthora* pathogens.
- The CAD7 subfamily has expanded in plant genomes but lost the lignin biosynthetic activity of canonical CAD subfamilies. In turn, we identified CAD7s as negative regulators of plant immunity that are induced by *Phytophthora* infection. Moreover, AtCAD7 was stabilized by Avr3a-like effectors and involved in suppression of pathogen-associated molecular pattern -triggered immunity, including callose deposition, ROS burst, and *WRKY33* expression.
- Our results reveal CAD7 subfamily proteins as negative regulators of plant immunity that are exploited by multiple Avr3a-like effectors to promote infection in different host plants.

Keywords: Avr3a, CAD7, host target, *Phytophthora*, plant immunity, RXLR effector

Introduction

Oomycetes are eukaryotic microbes that resemble filamentous fungi in morphology and physiology but belong to the kingdom Stramenopila (Tyler, 2001). Oomycetes include many destructive plant pathogens (Kamoun *et al.*, 2015), such as the notorious *Phytophthora infestans* that caused the Irish potato famine (Haas *et al.*, 2009), and the broad-host-range pathogen *Phytophthora capsici* that can infect at least 71 species of cultivated plants and weeds representing 27 families of plants, including tomato, pepper, cucurbits, and *Nicotiana* species (Granke *et al.*, 2012; Lamour *et al.*, 2012).

Plants have evolved an innate immune system that contains at least two principal overlapping layers of defense (Jones & Dangl, 2006). The first one is pattern-triggered immunity (PTI), which relies on plasma membrane-localized pattern recognition receptors (PRRs) to perceive apoplastic effectors (de Wit, 2016; Wang & Wang, 2018; Wang *et al.*, 2018) and microbe-associated molecular patterns (MAMPs; e.g. the lipid-binding elicitin protein, INF1). The second layer of plant immunity relies on the nucleotide-binding domain and leucine-rich repeat (NB-LRR)-type immune receptors to perceive pathogen effectors within the plant cytoplasm. It is formerly known as gene-for-gene resistance and now termed effector-triggered immunity (ETI) (Flor, 1971; Jones & Dangl, 2006; Boller & He, 2009).

One component of defense responses has been identified as cinnamyl alcohol dehydrogenases (CADs) that contribute to structural lignification during development. In addition, a number of them are strongly induced during infection and are involved in localized lignification as a barrier against infection. In *Arabidopsis*, nine genes have been annotated as encoding cinnamyl alcohol dehydrogenases (AtCAD1-9) (Costa *et al.*, 2003). Only AtCAD4 and AtCAD5 were confirmed as having significant activity against cinnamyl aldehydes (Kim *et al.*, 2004). *Arabidopsis* double mutants lacking *AtCAD4* and *AtCAD5* exhibit a limp floral stem with 40% reduction of lignin (Sibout *et al.*, 2005) and also are more susceptible to infection (Tronchet *et al.*, 2010). The close paralogs, AtCAD7 and AtCAD8 (previously called ELI3-1 and ELI3-2) were shown to be strongly induced by pathogens and pathogen-derived elicitors (Kiedrowski *et al.*, 1992). AtCAD8 (ELI3-2) was shown to be preferentially active towards 2-methoxybenzaldehyde, with much weaker activity against 3-methoxybenzaldehyde, salicylaldehyde, benzaldehyde and cinnamaldehyde (Somssich *et al.*, 1996; Vega-Arreguin *et al.*, 2014). A closely related potato CAD-like protein, DRD-1, was also strongly induced by infection or wounding, and exhibited broad specificity towards aromatic and aliphatic aldehydes with the lowest K_m towards 2-methoxybenzaldehyde, salicylaldehyde and hexanal (Montesano *et al.*, 2003). The preferred substrates of AtCAD1-3, 6 and 9 have not been clearly identified (Kim *et al.*, 2004). On the basis of patterns of tissue-specific gene expression, AtCAD1, 6, 7, 8 and 9 were identified as perhaps contributing in a minor way to developmental lignification, while AtCAD2 and AtCAD3 did not appear to be associated with lignification (Kim *et al.*, 2007).

PiAvr3a and its homologs in *P. sojae* (PsAvr1b, PsAvh1, PsAvh4 and PsAvh5) and *P. capsici* (PcAvr3a1 to PcAvr3a14) are all Avr3a-like effectors (Shan *et al.*, 2004; Armstrong *et al.*, 2005; Bos, 2007; Jiang *et al.*, 2008) with a similar structure (Boutemy *et al.*, 2011; Win *et al.*, 2012; Sun *et al.*, 2013). *PiAvr3a* contributes to the virulence of *P. infestans* (Armstrong *et al.*, 2005; Bos *et al.*, 2006; Bos *et al.*, 2010). It can suppress two BAK1/SERK3-dependent PTI responses, INF1-triggered cell death (ICD) and flg22-triggered immunity (Chaparro-Garcia *et al.*, 2011; Chaparro-Garcia *et al.*, 2015). *PiAvr3a*^{KI} and *PiAvr3a*^{EM} are two alleles of *PiAvr3a*. PiAvr3a$^{\mathrm{KI}}$ can be recognized by potato resistance protein R3a while PiAvr3a$^{\mathrm{EM}}$ evades recognition (Armstrong *et al.*, 2005). To date, two host targets of PiAvr3a have been reported. One is a host E3 ubiquitin ligase CMPG1, which is required for ICD and stabilized by PiAvr3a$^{\mathrm{KI}}$ (Bos *et al.*, 2010). The second is the plant GTPase Dynamin-related protein 2 (DRP2), which is involved in immune receptor-mediated endocytosis and required for FLS2 internalization (Chaparro-Garcia *et al.*, 2015). Recently we found that PcAvr3a12, an Avr3a-like effector from *P. capsici*, could enhance *Arabidopsis* susceptibility to *P. capsici* and specifically target the host peptidyl-prolyl cis-trans isomerase FKBP15-2 to suppress endoplasmic reticulum-mediated plant immunity (Fan *et al.*, 2018). While it indicates the diversity of host proteins targeted by Avr3a-like effectors, it remains largely unknown whether they also have common targets.

In this study, we found that Avr3a-like effectors are widely distributed across the genus *Phytophthora*. We screened for host proteins targeted by multiple *Phytophthora* Avr3a-like effectors, and found that related cinnamyl alcohol dehydrogenase-like proteins from *Arabidopsis thaliana* (AtCAD7) and *Nicotiana benthamiana* (NbCAD7) interacted with Avr3a-like effectors from *P. capsici*, *P. infestans* and *P. sojae*. Furthermore, we found evidence that both AtCAD7 and NbCAD7 could act as negative regulators of plant innate immunity, and that this activity doesn’t require the putative enzyme active site residues of these proteins.

Materials and Methods

Strains and plant materials

Agrobacterium GV3101 was used for transient expression, stable transformation, and virus-induced gene silencing (VIGS) experiments. *Saccharomyces cerevisiae* strains AH109 and Y187 were used for yeast transformation and mating. For inoculation in *Arabidopsis*, oomycete pathogen *P. capsici* strain LT263 was used.

For *Arabidopsis* transformation, wild-type Col-0 was used. *Agrobacterium*-mediated transformation was performed as previously described (Zhang *et al.*, 2006). All plants were grown at 23 ºC under a 13-hour light/11-hour dark cycle.

Plasmid construction

For over-expression, the entire ORFs of *AtCADs* were amplified by PCR and cloned into pART27 (Gleave, 1992) with *Kpn* I and *Cla* I. For BiFC, the new GATEWAY vectors (Gehl *et al.*, 2009) were used. For yeast-two-hybrid assays (Y2H), all effectors (without signal peptide) were amplified by PCR and cloned into pGBKT7 while *AtCAD* family members were cloned into pGADT7. To generate VIGS constructs, a 300-bp fragment of *NbCAD7* was amplified from *N. benthamiana* cDNA and cloned into the binary vector pTRV2, while TRV2::*GFP* was constructed as a control. All constructs were sequenced at GenScript (Nanjing, China). All primers used for plasmid constructions are listed in Table S1.

Yeast-two-hybrid assay

To screen for the effector targets, a cDNA library was prepared with the infected *Arabidopsis* leaves using *P. parasitica* strain Pp016 at 2 days post infiltration. Y2H screening was performed using the Matchmaker™ Gal4 Two-Hybrid System 3 (Clontech) as described in the manual.

Bimolecular fluorescence complementation assay (BiFC)

BiFC was performed using protocols described previously (Gehl *et al.*, 2009). We used the binary vectors pDEST-^{GW}VYNE, pDEST-VYNE(R)^{GW}, pDEST-^{GW}VYCE, and pDEST-VYCE(R)^{GW}. These vectors were transiently expressed in *N. benthamiana* and the florescence was observed 3 days after agroinfiltration.

Co-immunoprecipitation assay (Co-IP)

The proteins of *N. benthamiana* leaves expressing Co-IP constructs were extracted at 3 days post agro-infiltration, using lysis buffer (25 mM Tris-HCl pH 7.5; 150 mM NaCl; 1 mM EDTA; 0.5% NP-40) plus 2% W/V polyvinylpolypyrrolidone (PVPP), 1 mM dithiothreitol (DTT), and a protease inhibitor cocktail (Biotool). The total protein was incubated at 4 °C for 3 h with GFP-Trap_A beads (Chromotek, Germany). The beads were then washed with dilution buffer (10 mM Tris-HCl pH 7.5, 150 mM NaCl, and 0.5 mM EDTA). The resuspended GFP-Trap_A beads were boiled for 10 min at 95°C to dissociate the immunocomplexes.

Western blotting

To detect BiFC proteins, the samples were extracted using lysis buffer (50 mM Tris-HCl pH 7.5, 150 mM NaCl, 1 mM EDTA, 1% TritonX-100, 1% sodium deoxycholate, 5 mM sodium fluoride, and 1 mM sodium orthovanadate), plus 2% W/V PVPP, 5 mM DTT, and a protease inhibitor cocktail. For stabilization experiments, the samples were extracted using lysis buffer (25 mM Tris-HCl pH 7.5, 150 mM NaCl, 1 mM EDTA, and 0.5% NP-40) plus 2% W/V PVPP, 1 mM DTT, and a protease inhibitor cocktail. SDS–PAGE (SDS–polyacrylamide gel electrophoresis) was performed with proteins. Antibodies (anti-HA, anti-Myc, anti-FLAG, anti-mCherry, anti-GFP, goat anti-mouse and anti-rabbit) were used according to manual description.

Transient expression analysis

Agrobacterium transient expression assay was carried out on 4-6-week-old *N. benthamiana*. The agroinfiltration medium consisted of 10 mM $MgCl_2$, 10 mM MES, and 150 mM acetosyringone. *Agrobacterium* strain GV3101 with a final OD_{600} values of 0.2 to 0.4 in agroinfiltration medium was used. Transient expression assays in *Arabidopsis* protoplasts were performed as described (Yoo *et al.*, 2007).

qRT-PCR analysis

For all RT-PCR analysis, cDNA was synthesized with PrimeScript™ RT reagent Kit with gDNA Eraser (TaKaRa, China), and PCR reactions were performed with FastStart Universal SYBR Green Master according to the manufacturer's instructions (Roche, USA). *AtUBC9* was used as a reference gene in *Arabidopsis* for normalization. *NbEF1α* was used as a reference gene in *N. benthamiana* for normalization. All primers used for qRT-PCR are listed in Table S1.

VIGS analysis

VIGS was performed using a previously described method (Liu *et al.*, 2002). For *NbCAD7* silencing, a 300-bp fragment of *NbCAD7* was designed using the SGN VIGS tool (Fernandez-Pozo *et al.*, 2015) to ensure both efficiency and specificity of silencing. The *NbCAD7* fragment was cloned into TRV2 and a TRV2 vector containing a *GFP* fragment was used as a control. To choose the proper leaves for the following analysis, *PDS*-silenced plants were used to monitor the silencing effect. Infiltration of agrobacterium cultures containing TRV1 and TRV2 was performed on the lower leaves of 6-leaf stage *N. benthamiana*. The agroinfiltration medium of TRV1 and TRV2 were mixed in 1:1 ratio and a final concentration of $OD_{600} = 0.3$ was used. The VIGS plants were used for further analysis 3-5 weeks after infiltration.

Inoculation analysis

For *Arabidopsis* inoculation, about 800-1200 zoospores prepared from *P. capsici* strain LT263 were used to infect the 4-week-old leaves. For *N. benthamiana* inoculation, 0.3 cm^2 mycelium plugs cut from the *P. capsici* strain LT263 cultures, or about 800 zoospores prepared from *P. infestans* strain Pc21336 (lab strain isolated in China, virulent on R3 plant) were used to infect the VIGS plants.

Confocal microscopy

Imaging was conducted on an Olympus FV1000 confocal microscope using HCX APO L 10x/0.4, 20x/0.75, and 40x/0.95 water-dipping lenses. GFP and YFP were excited at 488 nm and detected at 500-540 nm. For mCherry observation, fluorescence was excited at 559 nm and detected at 580-630 nm.

Histochemical analysis

Two-month-old *Arabidopsis* stems were used for histochemical analysis. The basal part of the stem was sectioned by hand and then stained. Wiesner and Maule reactions were performed according to standard protocols (Sibout *et al.*, 2005).

Callose deposition and ROS burst analyses

Four-week-old *Arabidopsis* leaves treated with 1 μM flg22 were used for all analyses. Both callose deposition and ROS burst were assayed as previously described (Luna *et al.*, 2011; Sang & Macho, 2017).

Sequence and phylogenetic analysis

To identify the Avr3a-like sequences in oomycetes (Dataset S1), PiAvr3a, PsAvr1b, PsAvh5, PcAvr3a4, PcAvr3a11, and PcAvr3a12 were used to search the oomycete genomes via tBLASTn with an e-value cut-off of e-20. To identify the CAD homologs in plants (Dataset S2), AtCAD1-9 were used to search the plant proteins via blastp with an e-value cut-off of e-25. The protein sequences were aligned with M-Coffee (Wallace *et al.*, 2006) (Avr3a-like) or ClustalW2 (Larkin *et al.*, 2007) (CAD), and the phylogenetic relationships were inferred by PhyML (Guindon *et al.*, 2010). The trees were visualized by FigTree (http://tree.bio.ed.ac.uk/software/figtree).

Results

Avr3a-like proteins are distributed widely across the genus *Phytophthora*

To gain a comprehensive view of the distribution of Avr3a-like proteins in oomycetes, we used the sequences of the effectors PiAvr3a (Armstrong *et al.*, 2005; Bos *et al.*, 2006; Bos *et al.*, 2010), PsAvr1b (Shan *et al.*, 2004; Dou *et al.*, 2008), PsAvh5 (Sun *et al.*, 2013), PcAvr3a4 (Yaeno *et al.*, 2011), PcAvr3a11 (Boutemy *et al.*, 2011) and PcAvr3a12 (Fan *et al.*, 2018) to search oomycete genomes available in GenBank using tBLASTn with an E-value cutoff of e-20. One to 14 sequence matches were observed in the genomes of 10 surveyed species representing clades 1, 2, 4, 7, 8, and 10 (Kroon *et al.*, 2012) in *Phytophthora* (Fig. 1a). No sequence matches with an E-value better than e-20 were observed outside the genus *Phytophthora*, including downy mildews, *Phytopythium* and *Pythium* species. A phylogenetic tree of the Avr3a-like protein sequences (Fig. 1b) revealed two broad sub-families, one containing PsAvh5, and the other containing PiAvr3a, PsAvr1b, and the three *P. capsici* proteins used as queries. The Avh5 subfamily contained members from all species except *P. kernoviae*, while the PiAvr3a-PsAvr1b subfamily was missing representatives from *P. brassicae, P. ramorum*, and *P. cinnamomi*. Large species-specific gene family expansions have occurred in *P. capsici* (10 members), *P. megakarya* (6 members) and *P. palmivora* (5 members), while smaller expansions (2-4 members) have occurred in *P. infestans*, *P. sojae*, and *P. kernoviae.* All the Avr3a-like genes in *P. capsici*, except *PcAvr3a16*, *PcAvr3a17* and *PcAvr3a18*, organized in a single 187 kb cluster within the PacBio assembly of LT263 (Fig. S1), indicating that they may arise from tandem duplication events.

We used qRT-PCR to assay the transcript levels of *PcAvr3a1*, *PcAvr3a3*, *PcAvr3a5*, *PcAvr3a6*, *PcAvr3a11*, *PcAvr3a12*, and *PcAvr3a14* relative to *PcActin-like* genes during leaf infection of its host plants *Arabidopsis* and *N. benthamiana*. (Fig. S2). The results revealed that *PcAvr3a14* exhibited the highest transcript levels during early infection of *Arabidopsis* leaves (up to 100% of *PcActin* levels at 3-6 hpi), while *PcAvr3a3* showed the highest transcript levels during early infection of *N. benthamiana* leaves, up to 350% of *PcActin* at 3 hpi. *PcAvr3a5* exhibited moderate transcript levels during *Arabidopsis* infection (up to 10% of *PcActin* over 3-12 hpi) while *PcAvr3a1*, *PcAvr3a5*, *PcAvr3a12* and *PcAvr3a14* exhibited moderate transcript levels during *N. benthamiana* infection (up to 80% of *PcActin* over 3-24 hpi). Transcripts of *PcAvr3a6* and *PcAvr3a11* could barely be detected during infection of either plant.

Multiple *Phytophthora* Avr3a-like effectors interact with AtCAD7

Considering the structural conservation and partial sequence conservation of Avr3a-like effectors in *Phytophthora* spp. (Fig. 1, S3) we examined if there were host proteins targeted by multiple Avr3a family members. We screened a cDNA library prepared from *Phytophthora parasitica*-infected *Arabidopsis* leaves with PiAvr3a^{KI} and PsAvr1b using a yeast two-hybrid (Y2H) assay. Our analysis (Fig. 2a) revealed that both PiAvr3a^{KI} and

PsAvr1b interacted with AtCAD7. We thus hypothesized that AtCAD7 might be targeted by other Avr3a-like effectors. To test this hypothesis, we examined the interactions of AtCAD7 with several other Avr3a-like effectors, including PiAvr3a^{EM}, PcAvr3a1, and PcAvr3a12 (PcAvr3a12a) by pairwise Y2H. Consistently, all these effectors interacted with AtCAD7 in the Y2H assay while the non-Avr3a-like RXLR effector PITG_23129 from *P. infestans* did not (Fig. 2a).

To retest the interactions in plant cells, we employed bimolecular fluorescence complementation (BiFC) assays. The effectors (PsAvr1b, PiAvr3a^{KI}, PiAvr3a^{EM}, PcAvr3a1, PcAvr3a12, and the control PITG_23129) were fused with the N-terminal fragment of YFP (YFP^{N}) and AtCAD7 was fused with the C-terminal fragment of YFP (YFP^{C}). All these YFP fragment-fused proteins were successfully expressed as verified by western blotting (Fig. S4). Confocal microscopic observations revealed that the Avr3a-like effectors fused to YFP^{N} and AtCAD7 fused to YFP^{C} complemented to produce YFP fluorescence in *N. benthamiana* (Fig 2b), while the control *PITG_23129* did not (Fig. 2b). These results suggested that AtCAD7 could bind to the Avr3a-like effectors *in planta*.

We next extended the examination of Avr3a family proteins to PcAvr3a3, PcAvr3a5, PcAvr3a6, PcAvr3a11, and PcAvr3a14, using Y2H and BiFC assays (Fig. 3a-b). Both the Y2H and BiFC assays indicated interactions of AtCAD7 with PcAvr3a3, PcAvr3a5 and PcAvr3a6. However, PcAvr3a11 and PcAvr3a14 showed weak or inconsistent evidence, respectively, for interactions with AtCAD7.

We then used Co-IP assays to further validate the interactions of the PcAvr3a-like proteins with AtCAD7. Myc-tagged AtCAD7 was co-expressed in *N. benthamiana* with GFP fusions of each of the PcAvr3a-like proteins, then the effector proteins were recovered onto GFP-Trap A beads, and the presence of AtCAD7 was determined by western blotting with anti-Myc antibodies. The results (Fig. 3c) confirmed strong interactions of AtCAD7 with

PcAvr3a1, PcAvr3a6, and PcAvr3a12. PcAvr3a11 showed no interaction while PcAvr3a3, PcAvr3a5 and PcAvr3a14 showed weaker interactions.

The *CAD7* sub-family is expanded in plant genomes

Since *N. benthamiana* is a host for *P. capsici* and also for *P. infestans*, we were interested to determine whether CAD7 proteins from *N. benthamiana* could be bound by Avr3a-like effectors from these two pathogens. We first conducted a genome-wide analysis to determine the distribution of CAD7 homologs in the genomes of *N. benthamiana* and other plant species. As expected (Boerjan *et al.*, 2003), we found that CAD family proteins were conserved from moss to higher land plants. The proteins were distributed into 5 clades (Fig. S5). The *Arabidopsis* CADs fell into four of the clades, with AtCAD4 and 5 together, AtCAD2, 3 and 9 together, AtCAD6, 7 and 8 together, and AtCAD1 alone.

Interestingly, we observed that the CAD7 subfamily, containing AtCAD6, 7 and 8, was expanded in several plant genomes (Fig. S5). The CAD7 sub-family has 8 members in rice, 4 in maize, 8 in poplar, 3 in *Arabidopsis*, 7 in soybean, 15 in *N. benthamiana*, 9 in potato, 7 in tomato, and 4 in pepper. In contrast, in the *N. benthamiana* genome, non-CAD7 clades comprised only 6 members in total. Multiple co-orthologs of AtCAD7 and 8 were encoded in *N. benthamiana* (marked with blue dots in Fig. S5). These co-orthologs grouped into six sub-clades (7c1 to 7c6). Using bidirectional-best BLAST searches and OrthoMCL (Li *et al.*, 2003), we identified NbCAD7 (Niben101Scf02907g06016.1) in clade 7c1 as the closest ortholog of AtCAD7 and 8.

Since *AtCAD7* and *AtCAD8* were reported to be induced by bacterial and by fungal elicitors (Schmelzer *et al.*, 1989; Kiedrowski *et al.*, 1992; Trezzini *et al.*, 1993), we tested whether transcript levels of *AtCAD7*, *AtCAD8* and also *AtCAD6* were elevated during oomycete infection. Using qRT-PCR, we observed that *AtCAD6* levels were increased just under four-fold at 12 h post inoculation, *AtCAD7* transcripts were elevated over four-fold by 24 h post infection, and *AtCAD8* transcripts were elevated over five-fold by 60 h post inoculation (Fig. S6a-c). These observations were reinforced by using transgenic *Arabidopsis* plants carrying the beta-glucuronidase gene (*GUS*) driven by the promoters of *AtCAD6*, *7* and *8* (Fig. S6d-f). Thus transcripts of all three *Arabidopsis* genes in the *CAD7* clade appeared to be moderately increased by *P. capsici* infection.

Since *AtCAD6* and *AtCAD8* transcript levels were elevated during infection along with *AtCAD7*, and share sequence similarity with *AtCAD7*, we used a Y2H assay to test AtCAD6 and AtCAD8 proteins for interactions with PcAvr3a1, PcAvr3a3, PcAvr3a11, and PcAvr3a12. The results suggested that AtCAD6 could interact with PcAvr3a12, but that AtCAD8 could not interact with any of the four effectors (Fig. S7).

Targeting of NbCAD7 by *P. capsici* and *P. infestans* Avr3a-like effectors

To test if *N. benthamiana* co-orthologs of AtCAD7 could interact with Avr3a-like effectors from *P. capsici* and *P. infestans*, we selected NbCAD7 as a representative co-ortholog and used Y2H, BiFC, and Co-IP assays to test its interactions with the effectors. While the BiFC assays suggested that NbCAD7 might interact with all of the effectors tested (Fig. 3d,g), only the interactions of NbCAD7 with PcAvr3a12 and PiAvr3aEM were confirmed by both Co-IP (Fig. 3f,h) and Y2H (Fig. 3e,i). PiAvr3aKI showed a weaker interaction by Co-IP and none by Y2H (Fig 3e,i).

To investigate whether the CAD7 proteins and Avr3a-like effectors exhibited similar subcellular distributions, we co-expressed GFP-AtCAD7 and GFP-NbCAD7 with mCherry-PcAvr3a1 and mCherry-PcAvr3a12, respectively, in *N. benthamiana*. All fusion proteins were expressed and intact in plant cells as determined by western blotting (Fig. S8a). Confocal microscopic examination showed that mCherry-PcAvr3a1 and mCherry-PcAvr3a12 both showed the same distributions in the cytoplasm and nucleus of plant cells as the two GFP-CAD7 proteins (Fig. S8b-c). Thus the distributions of the CAD7 and Avr3a-like effector proteins were consistent with the possibility that they interact with each other.

Silencing of *AtCAD7* and *NbCAD7* attenuates *Phytophthora* infection

To explore the function of the *AtCAD7* gene during *P. capsici* infection, we analyzed *Arabidopsis* T-DNA insertion mutant lines of *AtCAD7*. Unfortunately, RT-PCR verification showed that the T-DNA insertion line (SALK_083037C) in the promoter of *AtCAD7* did not affect *AtCAD7* expression (data not shown). We therefore silenced *AtCAD7* in *Arabidopsis* stable RNAi lines. Two silenced lines, Ri.1 and Ri.2 showed 97% and 76% silencing of *AtCAD7*, based on qRT-PCR assays (Fig. 4a) whereas the transcript levels of *AtCAD6*, *AtCAD8*, and *AtCAD5* were not significantly affected (Fig. S9a-c). Neither Ri.1 nor Ri.2 showed any phenotypic defects in growth (Fig. S10a). When inoculated with *P. capsici*, the lesions at 2 dpi were slightly (20%) but significantly (*P*-value < 0.001) smaller on the RNAi plants as compared to the wild type Col-0 (Fig. 4b-c).

To test the function of *NbCAD7* during *P. capsici* and *P. infestans* infection of *N. benthamiana*, we silenced *NbCAD7* using VIGS. Due to the high sequence similarity among the co-orthologs of *NbCAD7*, it was difficult to silence *NbCAD7* exclusively. To minimize off-target silencing, a 300-bp fragment of *NbCAD7* was designed using the SGN VIGS tool (Fernandez-Pozo *et al.*, 2015). Nevertheless, after agro-infiltration, qRT-PCR examination showed that *NbCAD7* (Fig. 4d) and also the three closest paralogs in clade 7c1, *NbCAD1*, *NbCAD2*, and *NbCAD5* (Fig. S9d-f) were silenced in plants expressing TRV::*NbCAD7* (*tNb7*) as compared to plants expressing the control TRV::*GFP* (*tGFP*) construct. In contrast, *NbCAD18*, the ortholog of *AtCAD5*, was unaffected (Fig. S9g). The *tNb7* plants showed a decreased growth rate as compared to control plants *tGFP* (Fig. S10b). Trypan blue staining showed that both *P. capsici* and *P. infestans* colonization in the *tNb7* leaves was noticeably reduced, as compared to the control *tGFP* leaves (Fig. 4e-f). The *P. capsici* lesion diameters were slightly (9%) but significantly (*P*-value < 0.05) smaller in leaves expressing TRV::*NbCAD7* as compared to the tGFP control (Fig. 4g), while the *P. infestans* lesions were 47% smaller (*P*-value < 0.001) (Fig. 4h). Taken together, these results suggested that *CAD7* silencing in *Arabidopsis* and *N. benthamiana* slightly reduced susceptibility against *P. capsici* and *P. infestans*.

Overexpression of *AtCAD7* in *Arabidopsis* enhances *P. capsici* colonization

To further examine the function of *AtCAD7* during *Phytophthora* infection, we next overexpressed *AtCAD7* in *Arabidopsis*. After qRT-PCR screening, two independent lines (OE7.7 and OE7.9) with significant elevation of *AtCAD7* transcript levels (Fig. 5a) were selected for further analyses. Neither line showed developmental phenotypes compared to the wild type (WT) plants (Fig. S10c). Inoculation tests with *P. capsici* showed that pathogen colonization was increased in OE7 plants as compared to WT (Fig. 5b) and *P. capsici* lesions diameters in OE7 leaves were 38% larger (*P*-value < 0.01) than those in WT plants (Fig. 5c). Concordantly, qPCR results indicated that the *P. capsici* biomass was significantly (*P*-value <0.001) increased in OE7 plants, 3.6-fold in the case of OE7.7 (Fig. 5d). Taken together with the results from the *AtCAD7* silencing plants, these results suggested that *AtCAD7* supports *Phytophthora* infection and might function as a negative regulator of plant defense against *P. capsici*.

In contrast to AtCAD7, transient over-expression of NbCAD7 in *N. benthamiana* leaves did not result in a significant increase in *P. capsici* lesion size (Fig. S11), perhaps because the leaves already produced an over-abundance of NbCAD proteins.

Mutations in the predicted enzyme activity sites of AtCAD7 do not abolish its supportive function in *P. capsici* infection

Although AtCAD7 has a very low enzymatic activity *in vitro* towards cinnamyl aldehydes as compared to AtCAD5 (Kim *et al.*, 2004), its close paralog, AtCAD8, does have substantial activity towards 2-methoxybenzaldehyde (Somssich *et al.*, 1996). To test whether the predicted enzymatic activity sites of AtCAD7 were necessary for its interactions with Avr3a-like effectors and its negative role in plant defense against *Phytophthora*, we generated plants carrying two independent mutations (Fig. 6a) that abolish two different sets of key residues predicted to be required for enzyme activity (Bomati & Noel, 2005; Youn *et al.*, 2006) (Fig. S12). AtCAD7m1 (AtCAD7$^{C46A, T48A, S51A}$) abolishes residues predicted to be required for the binding of catalytic Zn^{2+}, $NADP^{+}$, and substrates, while AtCAD7m2 (AtCAD7$^{S210A, T211A, S212A, K215A}$) disrupted the predicted $NADP^{+}$-binding residues of AtCAD7. BiFC assays showed that both mutants interacted with PcAvr3a5, PcAvr3a12 and PcAvr3a14 as observed with wild-type AtCAD7 (Fig. 6b-c). Co-IP assays confirmed that AtCAD7m2 interacted with all three Avr3a-like effectors (Fig. 6d) as observed for WT AtCAD7 (Fig. 3c) (i.e. strongly with PcAvr3a12, and weakly with PcAvr3a5 and PcAvr3a14). We thus conclude that the predicted key enzyme activity sites of AtCAD7 are not required for its interactions with the tested Avr3a-like effectors.

We next generated *Arabidopsis* lines expressing *AtCAD7m1* (OE7m1) or *AtCAD7m2* (OE7m2) (Fig. 6e) driven by the 35S promoter. Similar to OE7, OE7m1 and OE7m2 plants did not show any phenotypic changes in development (Fig. S10c). Neither set of mutations noticeably altered the ability of *AtCAD7* over-expression to increase susceptibility to *P. capsici* infection (Fig. 6f-h). Thus, we conclude that the ability of AtCAD7 to promote *P. capsici* infection does not require its putative enzymatic activity.

To analyze the contribution of *AtCAD7* to lignification in *Arabidopsis*, we performed lignin staining with the sectioned stems of *AtCAD7*-silenced *Arabidopsis* lines Ri.1 and Ri.2. Both Wiesner (Fig. S13a) and Maule (Fig. S13b) staining reactions showed that stem xylems of Ri plants had staining patterns similar to the WT plants. This confirmed earlier studies on the minor function of AtCAD7 in lignification (Kim *et al.*, 2004; Kim *et al.*, 2007) and indicated that *AtCAD7* silencing had no noticeable impact on xylem lignification. In addition, we also stained the inflorescence stems of the *Arabidopsis* over-expression lines, OE7 and OE7m, with the WT plants as controls. Consistently, the dye intensities and staining patterns of all xylem tissues visualized by the Wiesner (Fig. S13c) and Maule (Fig. S13d) reactions did not show any differences. We thus conclude that the contribution of AtCAD7 to lignin biosynthesis is, at most, minor (Kim *et al.*, 2004).

NbCAD7 amplifies the suppression of INF1-triggered cell death by PiAvr3a^{KI}

Considering that PiAvr3a^{KI} could suppress INF1-triggered plant immunity (Bos *et al.*, 2006), we performed cell death assays in *NbCAD7*-silenced plants (*tNb7*) and control plants (*tGFP*) to investigate the role of NbCAD7 in INF1-triggered immunity. To measure the severity of cell death more precisely, we defined three cell death grades for treated *N. benthamiana* leaves (Fig. 7a). Constructs carrying *INF1* were agro-infiltrated into *N. benthamiana* plants which had previously been inoculated with *tNb7* and *tGFP* constructs, and the cell death occurrence was recorded. ICD appeared in *tNb7* leaves but not in *tGFP* leaves at 2 days post infiltration (dpi) (Fig. 7b). Statistical analyses indicated that cell death triggered by INF1 was significantly (P-value < 0.001) increased in *tNb7* plants as compared to control plants *tGFP* (Fig. 7c) at 2 dpi. This result suggested that ICD was accelerated by silencing of *NbCAD7*. We thus concluded that NbCAD7 can suppress ICD. To further confirm this, we performed cell death assays in *N. benthamiana* leaves transiently overexpressing *NbCAD7* (Nb7OE) and in control leaves expressing *GFP* (GFP). Consistent with the results described above, cell death triggered by INF1 was attenuated in Nb7OE leaves as compared to the GFP leaves at 3 dpi (Fig. 7d-e). These results support that NbCAD7 can negatively regulate ICD. As shown in Fig. S14, transient expression of *AtCAD7* in *N. benthamiana* leaves could also negatively regulate ICD, and this ability was not significantly affected by mutations in the predicted enzyme active site of AtCAD7.

Based on the above results, we hypothesized that *NbCAD7* might modulate the suppression of ICD by PiAvr3a^{KI}. To test this hypothesis, constructs containing either *PiAvr3a*^{KI} or control *GFP* were co-expressed with *INF1* in *NbCAD7*-silenced plants (*tNb7*) and control plants (*tGFP*). Cell death was scored at 3 dpi. The results showed that PiAvr3a^{KI} suppressed 83% of the ICD in *tGFP* control plants, but to a significantly lesser extent (35%) in *tNb7* plants (Fig. 7f). This indicated that the suppression of ICD by PiAvr3a^{KI} was attenuated in *NbCAD7*-silenced plants. Therefore, our results revealed that the ability of PiAvr3a^{KI} to suppress ICD was correlated with the transcript levels of *NbCAD7*.

***AtCAD7* can suppress callose deposition, ROS burst, and *WRKY33* expression**

Considering that NbCAD7 could suppress ICD, we further examined the ability of *AtCAD7* to modulate innate immunity in *Arabidopsis*. Callose deposition in the plant cell wall is an important barrier against pathogen attack and is a hallmark of PTI triggered by MAMP molecules such as flg22 (Luna *et al.*, 2011). Treatment of *AtCAD7*-overexpression lines (OE7.7 and OE7.9) and *AtCAD7*-silencing lines (Ri.1 and Ri.2) with flg22 showed that callose deposition in leaves was significantly reduced in OE7 leaves and increased in Ri leaves as compared to wild-type (Fig. 7g). We also analyzed reactive oxygen species (ROS) levels, which represents an early PTI response (Baxter *et al.*, 2014; Mittler, 2017), using DAB staining. The analysis showed that in contrast to the ROS burst in wild-type plants, a reduced oxidative burst was observed in *AtCAD7*-overexpression lines while an increased burst was observed in *AtCAD7*-silencing lines (Fig. 7g). Statistical analyses across multiple leaves revealed that both callose deposition and ROS levels were significantly reduced in *AtCAD7*-overexpression lines but were enhanced in *AtCAD7*-silencing lines (Fig. 7h-i). To investigate if the expression of defense-related genes was affected by *AtCAD7* overexpression, we performed qRT-PCR assays (Fig. S15). This analysis revealed that among all PTI genes tested, *WRKY33*, a transcription factor gene involved in PTI signaling and defense against necrotrophs (Zheng *et al.*, 2006), showed greatly reduced transcript levels in *Arabidopsis* plants overexpressing *AtCAD7*. Taken together, these results indicated that *AtCAD7* could suppress flg22-triggered PTI responses.

AtCAD7 is stabilized by PiAvr3a and PcAvr3a12

The stability of several host targets of oomycete RXLR effectors is associated with the 26S proteasome (Bos *et al.*, 2010; Wang *et al.*, 2015). To explore whether Avr3a-like effectors could affect accumulation of AtCAD7 and whether the accumulation of AtCAD7 is modulated by the 26S proteasome, *A. tumefaciens* carrying constructs encoding Myc-tagged AtCAD7 was co-infiltrated into *N. benthamiana* along with *A. tumefaciens* carrying constructs encoding GFP-tagged Avr3a^{EM}, Avr3a^{KI}, PcAvr3a12, or a GFP control. 26S proteasome inhibitor MG132 or control dimethyl sulfoxide (DMSO) was injected at 36 hours after agro-infiltration (hai) and samples were harvested at 48 hai. In the absence of MG132, AtCAD7 showed increased accumulation in the effector-expressing leaves as compared to GFP-expressing leaves (Fig. 8). However, in the presence of MG132, effector expression did not affect AtCAD7 accumulation (Fig. 8). These results suggest that the effectors may increase the accumulation of AtCAD7 by inhibiting 26S proteasome-mediated degradation of AtCAD7. The increased AtCAD7-Myc protein accumulation in the effector-expressing plants was not due to an increased level of the RNA transcript (Fig. 8).

To further confirm the stabilization of AtCAD7 by Avr3a effectors in *Arabidopsis*, we examined the AtCAD7-Myc accumulation in the presence and absence of Avr3a effectors in *Arabidopsis* protoplasts. The result clearly showed that AtCAD7-Myc abundance was increased by PiAvr3a and PcAvr3a12 (Fig. S16). We also performed stabilization experiments with NbCAD7 in *N. benthamiana* but did not observe significantly increased NbCAD7 accumulation by Avr3a-like effectors.

Since it was previously identified that PiAvr3a targets and stabilizes the E3 ligase CMPG1 (Bos *et al.*, 2010), we examined if NbCAD7 interacted with NbCMPG1 directly. Both Y2H and BiFC assays showed that there was no direct interaction between them (Fig. S17a-b), suggesting an independent interaction of PiAvr3a with NbCAD7 and NbCMPG1. Also, PcAvr3a12 is unlikely to interact with NbCMPG1a or NbCMPG1b, as revealed by Y2H and BiFC (Fig. S17c-d).

Discussion

Phytophthora spp. possesses a large number of RXLR effectors, that are fast evolving due to selection pressure imposed by the co-evolutionary conflict between pathogens and hosts (Dangl & Jones, 2001; Jones & Dangl, 2006). Despite the diversity of RXLR effectors, several families of effectors show substantial conservation across widely divergent species, including families defined by PsAvh238 (Wang *et al.*, 2011), PsAvh163 (Anderson *et al.*, 2012), HaAvh23/PsAvh73 (Deb *et al.*, 2018), and especially PiAvr3a (Bos, 2007; Vega-Arreguin *et al.*, 2014). The conservation of Avr3a-like effectors, across at least six *Phytophthora* clades, including the highly divergent *P. kernoviae*, suggests a particular significance for this family for pathogenicity on diverse hosts.

Here, we have shown, using Y2H, BiFC, and Co-IP assays, that several Avr3a-like effectors from *P. capsici* directly target the protein AtCAD7 in *Arabidopsis* and its closest homolog in *N. benthamiana*, NbCAD7 (Fig. 2-3). PiAvr3a has been previously shown to target the E3-ligase CMPG1 (Bos *et al.*, 2010) as well as the GTPase DRP2 (Chaparro-Garcia *et al.*, 2015). Furthermore, PcAvr3a12 has been shown to bind to AtFKBP15-2 to suppress endoplasmic reticulum-mediated plant immunity (Fan *et al.*, 2018). Our results here showed that NbCMPG1 did not bind to either NbCAD7 or PcAvr3a12, while PiAvr3a did not bind to FKBP15-2 (Fan *et al.*, 2018). Thus both PiAvr3a and PcAvr3a12 are revealed to have both shared and specific targets in host plants. These observations also suggest that individual oomycete RXLR effectors may have multiple physiologically relevant host target proteins. Mukhtar *et al* (2011) also noted numerous examples of effectors from the oomycete *Hyaloperonospora arabidopsidis* and the bacteria *Pseudomonas syringae* that bound multiple *Arabidopsis* target proteins in a Y2H screen.

Our phylogenetic analysis revealed that the CAD7 sub-family of cinnamaldehyde dehydrogenases, defined by AtCAD6, AtCAD7 and AtCAD8, has greatly expanded compared to the other CAD sub-families. Of these *AtCAD7* (*Eli3-1*) and *AtCAD8* (*Eli3-2*), as well as a parsley homolog, were previously reported to be strongly induced by *P. sojae* elicitors (Gleave, 1992; Trezzini *et al.*, 1993) and by *Pseudomonas* infection (Kiedrowski *et al.*, 1992). Furthermore, *StuCAD6* (*DRD-1*), a closely related potato *CAD* gene, was reported to be strongly induced during *Erwinia* infection of potato (Montesano *et al.*, 2003). Our data showed, likewise, that *AtCAD6*, *AtCAD7* and *AtCAD8* transcript levels were strongly elevated during *P. capsici* infection of *Arabidopsis* leaves, albeit with different timing (Fig. S6). *AtCAD7* transcript levels exceeded *AtCAD6* levels at all time points (Fig. S6), suggesting that *AtCAD7* represented the most important response to early infection; Of the three tested AtCAD proteins, only AtCAD6 and AtCAD7 (but not AtCAD8) were targeted by

PcAvr3a-like proteins, thus suggesting that the early-induced AtCADs are the primary targets for PcAvr3a-like proteins. However, we cannot rule out that AtCAD8 (and other AtCAD proteins) might be targeted by other *P. capsici* RXLR effectors, including other PcAvr3a-like proteins that were not analyzed here.

Although cinnamaldehyde dehydrogenases are typically considered to function in lignin production, our data indicate that the CAD7 sub-family proteins primarily have roles as negative regulators of plant immunity. Silencing or over-expression of *AtCAD7* in *Arabidopsis* plants did not discernibly affect lignification (Fig. S13) but made the plants more resistant (Fig. 4) and or susceptible (Fig. 5) to *P. capsici*, respectively. Similarly, silencing of *NbCAD7* made *N. benthamiana* leaves more resistant to *P. capsici* and especially to *P. infestans* (Fig. 4), while over-expression did not produce a measurable increase in *P. capsici* lesion size under the conditions of the assay (Fig. S11). The deposition of callose and production of reactive oxygen species (ROS) were decreased significantly in the *AtCAD7*-overexpressed plants treated with PTI inducer flg22, while they were significantly increased in the *AtCAD7*-silenced plants (Fig. 7). Most strikingly, the transcript levels of the transcription factor *WRKY33* were reduced 3-4 fold in *Arabidopsis* plants over-expressing *AtCAD7* (Fig. S15). WRKY33 is a key transcription factor required for resistance of *Arabidopsis* against necrotrophs. It is involved in PTI signaling and defense against necrotrophs (Zheng *et al.*, 2006). Consistent with this, *N. benthamiana* homolog of WRKY33, WRKY8, is required for resistance against *P. infestans* and *Botrytis cinerea* (Ishihama *et al.*, 2011).

The negative regulatory role of the CAD7 proteins seems counter-intuitive, given their strong induction during infection. However, the induction of negative regulators during a defense response provides a mechanism to modulate or spatially restrict that response (Rodriguez *et al.*, 2016). Furthermore, Hillmer *et al* (2017) showed via a systems approach that negative feedback loops within plant defense signaling networks provide extensive buffering against interference by pathogen effectors (Tyler, 2017). Thus, pathogen effectors that target cinnamyl alcohol dehydrogenases to attack lignin biosynthesis might inadvertently stimulate defense if they also target CAD7 sub-family proteins; in this context, the CAD7 sub-family proteins could be considered decoys. Intriguingly however, *P. capsici* and *P. infestans* appears to have evolved Avr3a-like effectors that can exploit this negative feedback loop to the advantage of the pathogen, highlighting once again the relentless nature of the pathogen-plant arms race.

Our data show that over-expression of *NbCAD7* in *N. benthamiana* leaves could partially, but significantly, suppress ICD, while silencing of *NbCAD7* could accelerate ICD. Silencing of *NbCAD7* could also significantly reduce the suppression of ICD by PiAvr3a^{KI}. However, our data do not support the hypothesis that binding to NbCAD7 mediates the ability of PiAvr3a^{KI} to suppress ICD. For example, PcAvr3a12 and PiAvr3a^{EM} both interact with NbCAD7 more strongly in the Y2H assays than PiAvr3a^{KI}, yet neither effector can suppress ICD. Thus we speculate that, PiAvr3a^{KI} and NbCAD7 suppress ICD additively, or possibly synergistically, through different pathways. These observations are consistent with the finding that the binding of PiAvr3a^{KI} to a different target, CMPG1, is required for suppression of ICD (Bos *et al.*, 2010). On the other hand, we cannot rule out the possibility that the nature of the PiAvr3a^{KI}-NbCAD7 interaction is different than the interaction of NbCAD7 with the other Avr3a-like effectors. For example, the *Arabidopsis* RIN4 protein is a conserved target of bacterial effectors AvrB, AvrRPM1, and AvrRpt2, but while AvrB and AvrRPM1 induce phosphorylation of RIN4 (Mackey *et al.*, 2002). AvrRpt2 induces its post-transcriptional disappearance (Mackey *et al.*, 2003).

AtCAD7 and also AtCAD1, AtCAD6, AtCAD8 and AtCAD9, were previously reported to make, at most, minor contributions to lignification (Kim *et al.*, 2007), which is supported by our observations (Fig. S13). AtCAD8, which is closely similar to AtCAD7, was reported to exhibit 2-methoxybenzaldehyde dehydrogenase activity (Somssich *et al.*, 1996), as was StuCAD6 (DRD-1) (Montesano *et al.*, 2003). Furthermore, the two closest homologs of AtCAD7 in cucumber, CsCAD3 and CsCAD4, also preferred 2-methoxybenzaldehyde as a substrate (Varbanova *et al.*, 2011). Thus AtCAD7 and NbCAD7 might also exhibit 2-methoxybenzaldehyde dehydrogenase activity. However, our data indicate that the predicted active site residues of AtCAD7 are not required for its negative regulation of immunity. We speculate that this dual role of the AtCAD7 and NbCAD7 proteins may serve to coordinate immune function with lignification in lignifying tissues, perhaps to redirect the products of the phenylpropanoid pathway away from defense compounds.

The mechanism(s) by which Avr3a-like effectors exploit the negative regulatory function of CAD7 proteins to inhibit defense are not yet fully clear. Our data showed that over-expression of PiAvr3a^{KI}, PiAvr3a^{EM}, or PcAvr3a12 could stabilize co-expressed AtCAD7 protein in *N. benthamiana* leaves and *Arabidopsis* protoplasts, by inhibiting the degradation through 26S proteasome (Fig. 8, Fig. S16). However, co-expressed NbCAD7 protein was not detectably stabilized in a similar experiment. It is possible that the Avr3a-like effectors do indeed act to stabilize CAD7 proteins, but that features of the assay, including especially the presence of an abundance of endogenous NbCAD7-subfamily proteins, may obscure the full extent of the stabilization. On the other hand, it is plausible that binding of the effectors activates CAD7 function via other mechanisms, for example by stabilizing the binding of CAD7 to the target that it negatively regulates, or by displacing CAD7 from an inhibitor protein.

In summary, the Avr3a-like effectors could target and exploit CAD7, a negative regulator of plant innate immunity, to facilitate pathogen infection by suppressing plant PTI (Fig. 9).

Acknowledgments

We are grateful to Dr. Ming-Bo Wang, Dr. Jim Peacock, and Dr. Liz Dennis (CSIRO Agriculture and Food, Canberra, Australia), Dr. Francine Govers (Wageningen University, The Netherlands), and all the lab members for their insightful discussions in this study. This work was supported by China Agriculture Research System (CARS-09), National Natural Science Foundation of China (31125022 and 31561143007), the Programme of Introducing Talents of Innovative Discipline to Universities (project 111) from the State Administration of Foreign Experts Affairs (#B18042), BBSRC/EPSRC grant to WISB (BB/M017982/1), and China Postdoctoral Science Foundation (2017M623262).

Author contributions

W.S., T.L., Y.M., and Q.W. conceived and designed the experiments. T.L., R.F., Y. M., L.L., L.D. G.F., W.L., and G.H. performed the experiments. M.Z. constructed the cDNA library. B.M.T. designed the CAD7 mutants and surveyed the Avr3a-like effector family. P.S., Q.W., Y. M., and Y.D. were involved in data interpretation and supported T.L., B.M.T. and W.S. in writing the manuscript. All authors reviewed the manuscript.

References

Anderson RG, Casady MS, Fee RA, Vaughan MM, Deb D, Fedkenheuer K, Huffaker A, Schmelz EA, Tyler BM, McDowell JM. 2012. Homologous RXLR effectors from *Hyaloperonospora arabidopsidis* and *Phytophthora sojae* suppress immunity in distantly related plants. *Plant J* **72**: 882-893.

Armstrong MR, Whisson SC, Pritchard L, Bos JI, Venter E, Avrova AO, Rehmany AP, Bohme U, Brooks K, Cherevach I, et al. 2005. An ancestral oomycete locus contains late blight avirulence gene *Avr3a*, encoding a protein that is recognized in the host cytoplasm. *Proc Natl Acad Sci USA* **102**: 7766-7771.

Baxter A, Mittler R, Suzuki N. 2014. ROS as key players in plant stress signalling. *J Exp Bot* **65**: 1229-1240.

Boerjan W, Ralph J, Baucher M. 2003. Lignin biosynthesis. *Annu Rev Plant Biol* **54**: 519-546.

Boller T, He SY. 2009. Innate immunity in plants: an arms race between pattern recognition receptors in plants and effectors in microbial pathogens. *Science* **324**: 742-744.

Bomati EK, Noel JP. 2005. Structural and kinetic basis for substrate selectivity in *Populus tremuloides* sinapyl alcohol dehydrogenase. *Plant Cell* **17**: 1598-1611.

Bos JIB. 2007. *Function, structure and evolution of the effector Avr3a of Phytophthora infestans.* PhD Thesis, The Ohio State University USA.

Bos JIB, Armstrong MR, Gilroy EM, Boevink PC, Hein I, Taylor RM, Tian ZD, Engelhardt S, Vetukuri RR, Harrower B, et al. 2010. *Phytophthora infestans* effector AVR3a is essential for virulence and manipulates plant immunity by stabilizing host E3 ligase CMPG1. *Proc Natl Acad Sci USA* **107**: 9909-9914.

Bos JIB, Kanneganti TD, Young C, Cakir C, Huitema E, Win J, Armstrong MR, Birch PR, Kamoun S. 2006. The C-terminal half of *Phytophthora infestans* RXLR effector AVR3a is sufficient to trigger R3a-mediated hypersensitivity and suppress INF1-induced cell death in *Nicotiana benthamiana*. *Plant J* **48**: 165-176.

Boutemy LS, King SR, Win J, Hughes RK, Clarke TA, Blumenschein TM, Kamoun S, Banfield MJ. 2011. Structures of *Phytophthora* RXLR effector proteins: a conserved but adaptable fold underpins functional diversity. *J Biol Chem* **286**: 35834-35842.

Chaparro-Garcia A, Schwizer S, Sklenar J, Yoshida K, Petre B, Bos JI, Schornack S, Jones AM, Bozkurt TO, Kamoun S. 2015. *Phytophthora infestans* RXLR-WY effector Avr3a associates with dynamin-related protein 2 required for endocytosis of the plant pattern recognition receptor FLS2. *PLoS One* **10**: e0137071.

Chaparro-Garcia A, Wilkinson RC, Gimenez-Ibanez S, Findlay K, Coffey MD, Zipfel C, Rathjen JP, Kamoun S, Schornack S. 2011. The receptor-like kinase SERK3/BAK1 is required for basal resistance against the late blight pathogen *Phytophthora infestans* in *Nicotiana benthamiana*. *PLoS One* **6**: e16608.

Costa MA, Collins RE, Anterola AM, Cochrane FC, Davin LB, Lewis NG. 2003. An in silico assessment of gene function and organization of the phenylpropanoid pathway metabolic networks in *Arabidopsis thaliana* and limitations thereof. *Phytochemistry* **64**: 1097-1112.

Dangl JL, Jones JD. 2001. Plant pathogens and integrated defence responses to infection. *Nature* **411**: 826-833.

de Wit PJ. 2016. *Cladosporium fulvum* effectors: weapons in the arms race with tomato. *Annu Rev Phytopathol* **54**: 1-23.

Deb D, Anderson RG, How-Yew-Kin T, Tyler BM, McDowell JM. 2018. Conserved RXLR effectors from oomycetes *Hyaloperonospora arabidopsidis* and *Phytophthora sojae* suppress PAMP- and effector-triggered immunity in diverse plants. *Mol Plant Microbe Interact* **31**: 374-385.

Dou DL, Kale SD, Wang XL, Chen YB, Wang QQ, Wang X, Jiang RHY, Arredondo FD, Anderson RG, Thakur PB, et al. 2008. Conserved C-terminal motifs required for avirulence and suppression of cell death by *Phytophthora sojae* effector Avr1b. *Plant Cell* **20**: 1118-1133.

Fan G, Yang Y, Li T, Lu W, Du Y, Qiang X, Wen Q, Shan W. 2018. A *Phytophthora capsici* RXLR effector targets and Inhibits a plant PPIase to suppress endoplasmic reticulum-mediated immunity. *Mol Plant* **11**: 1067-1083.

Fernandez-Pozo N, Rosli HG, Martin GB, Mueller LA. 2015. The SGN VIGS tool: user-friendly software to design virus-induced gene silencing (VIGS) constructs for functional genomics. *Mol Plant* **8**: 486-488.

Flor HH. 1971. Current status of the gene-for-gene concept. *Annu Rev Phytopathol* **9**: 275-279.

Gehl C, Waadt R, Kudla J, Mendel RR, Hansch R. 2009. New GATEWAY vectors for high throughput analyses of protein-protein interactions by bimolecular fluorescence complementation. *Mol Plant* **2**: 1051-1058.

Gleave AP. 1992. A versatile binary vector system with a T-DNA organisational structure conducive to efficient integration of cloned DNA into the plant genome. *Plant Mol Biol* **20**: 1203-1207.

Granke LL, Quesada-Ocampo L, Lamour K, Hausbeck MK. 2012. Advances in research on *Phytophthora capsici* on vegetable crops in the United States. *Plant Disease* **96**: 1588-1600.

Guindon S, Dufayard JF, Lefort V, Anisimova M, Hordijk W, Gascuel O. 2010. New algorithms and methods to estimate maximum-likelihood phylogenies: assessing the performance of PhyML 3.0. *Syst Biol* **59**: 307-321.

Haas BJ, Kamoun S, Zody MC, Jiang RH, Handsaker RE, Cano LM, Grabherr M, Kodira CD, Raffaele S, Torto-Alalibo T, et al. 2009. Genome sequence and analysis of the Irish potato famine pathogen *Phytophthora infestans*. *Nature* **461**: 393-398.

Hillmer RA, Tsuda K, Rallapalli G, Asai S, Truman W, Papke MD, Sakakibara H, Jones JDG, Myers CL, Katagiri F. 2017. The highly buffered Arabidopsis immune signaling network conceals the functions of its components. *Plos Genetics* **13**: e1006639.

Ishihama N, Yamada R, Yoshioka M, Katou S, Yoshioka H. 2011. Phosphorylation of the *Nicotiana benthamiana* WRKY8 transcription factor by MAPK functions in the defense response. *Plant Cell* **23**: 1153.

Jiang RH, Tripathy S, Govers F, Tyler BM. 2008. RXLR effector reservoir in two *Phytophthora* species is dominated by a single rapidly evolving superfamily with more than 700 members. *Proc Natl Acad Sci USA* **105**: 4874-4879.

Jones JD, Dangl JL. 2006. The plant immune system. *Nature* **444**: 323-329.

Kamoun S, Furzer O, Jones JD, Judelson HS, Ali GS, Dalio RJ, Roy SG, Schena L, Zambounis A, Panabieres F, et al. 2015. The top 10 oomycete pathogens in molecular plant pathology. *Mol Plant Pathol* **16**: 413-434.

Kiedrowski S, Kawalleck P, Hahlbrock K, Somssich IE, Dangl JL. 1992. Rapid activation of a novel plant defense gene is strictly dependent on the *Arabidopsis* RPM1 disease resistance locus. *EMBO J* **11**: 4677-4684.

Kim SJ, Kim KW, Cho MH, Franceschi VR, Davin LB, Lewis NG. 2007. Expression of cinnamyl alcohol dehydrogenases and their putative homologues during *Arabidopsis thaliana* growth and development: lessons for database annotations? *Phytochemistry* **68**: 1957-1974.

Kim SJ, Kim MR, Bedgar DL, Moinuddin SG, Cardenas CL, Davin LB, Kang C, Lewis NG. 2004. Functional reclassification of the putative cinnamyl alcohol dehydrogenase multigene family in *Arabidopsis*. *Proc Natl Acad Sci USA* **101**: 1455-1460.

Kronmiller B, Tyler BM. 2019. High quality genome assembly of *Phytophthora capsici* strain LT263 produced from Pacific Bioscinces long reads. *Mol Plant Microbe Interact*: in preparation.

Kroon LP, Brouwer H, de Cock AW, Govers F. 2012. The genus *Phytophthora* anno 2012. *Phytopathology* **102**: 348-364.

Lamour KH, Stam R, Jupe J, Huitema E. 2012. The oomycete broad-host-range pathogen *Phytophthora capsici*. *Mol Plant Pathol* **13**: 329-337.

Larkin MA, Blackshields G, Brown NP, Chenna R, McGettigan PA, McWilliam H, Valentin F, Wallace IM, Wilm A, Lopez R, et al. 2007. Clustal W and Clustal X version 2.0. *Bioinformatics* **23**: 2947-2948.

Li L, Stoeckert CJ, Jr., Roos DS. 2003. OrthoMCL: identification of ortholog groups for eukaryotic genomes. *Genome Res* **13**: 2178-2189.

Liu YL, Schiff M, Marathe R, Dinesh-Kumar SP. 2002. Tobacco *Rar1*, *EDS1* and *NPR1/NIM1* like genes are required for N-mediated resistance to tobacco mosaic virus. *Plant Journal* **30**: 415-429.

Luna E, Pastor V, Robert J, Flors V, Mauch-Mani B, Ton J. 2011. Callose deposition: a multifaceted plant defense response. *Mol Plant Microbe Interact* **24**: 183-193.

Mackey D, Belkhadir Y, Alonso JM, Ecker JR, Dangl JL. 2003. *Arabidopsis* RIN4 is a target of the type III virulence effector AvrRpt2 and modulates RPS2-mediated resistance. *Cell* **112**: 379-389.

Mackey D, Holt BF, Wiig A, Dangl JL. 2002. RIN4 interacts with *Pseudomonas syringae* type III effector molecules and is required for RPM1-mediated resistance in *Arabidopsis*. *Cell* **108**: 743-754.

Mittler R. 2017. ROS are good. *Trends Plant Sci* **22**: 11-19.

Montesano M, Hyytiainen H, Wettstein R, Palva ET. 2003. A novel potato defence-related alcohol:NADP+ oxidoreductase induced in response to *Erwinia carotovora*. *Plant Mol Biol* **52**: 177-189.

Mukhtar MS, Carvunis AR, Dreze M, Epple P, Steinbrenner J, Moore J, Tasan M, Galli M, Hao T, Nishimura MT, et al. 2011. Independently evolved virulence effectors converge onto hubs in a plant immune system network. *Science* **333**: 596-601.

Rodriguez E, El Ghoul H, Mundy J, Petersen M. 2016. Making sense of plant autoimmunity and "negative regulators". *FEBS Journal* **283**: 1385-1391.

Sang Y, Macho AP. 2017. Analysis of PAMP-triggered ROS burst in plant immunity. *Methods Mol Biol* **1578**: 143-153.

Schmelzer E, Kruger-Lebus S, Hahlbrock K. 1989. Temporal and spatial patterns of gene expression around sites of attempted fungal infection in parsley leaves. *Plant Cell* **1**: 993–1001.

Shan W, Cao M, Leung D, Tyler BM. 2004. The *Avr1b* locus of *Phytophthora sojae* encodes an elicitor and a regulator required for avirulence on soybean plants carrying resistance gene *Rps1b*. *Mol Plant Microbe Interact* **17**: 394-403.

Sibout R, Eudes A, Mouille G, Pollet B, Lapierre C, Jouanin L, Seguin A. 2005. *CINNAMYL ALCOHOL DEHYDROGENASE-C* and *-D* are the primary genes involved in lignin biosynthesis in the floral stem of *Arabidopsis*. *Plant Cell* **17**: 2059-2076.

Somssich IE, Wernert P, Kiedrowski S, Hahlbrock K. 1996. *Arabidopsis thaliana* defense-related protein ELI3 is an aromatic alcohol:NADP(+) oxidoreductase. *Proc Natl Acad Sci USA* **93**: 14199-14203.

Sun F, Kale SD, Azurmendi HF, Li D, Tyler BM, Capelluto DG. 2013. Structural basis for interactions of the *Phytophthora sojae* RxLR effector Avh5 with phosphatidylinositol 3-phosphate and for host cell entry. *Mol Plant Microbe Interact* **26**: 330-344.

Trezzini GF, Horrichs A, Somssich IE. 1993. Isolation of putative defense-related genes from *Arabidopsis thaliana* and expression in fungal elicitor-treated cells. *Plant Molecular Biology* **21**: 385-389.

Tronchet M, Balague C, Kroj T, Jouanin L, Roby D. 2010. Cinnamyl alcohol dehydrogenases-C and D, key enzymes in lignin biosynthesis, play an essential role in disease resistance in *Arabidopsis*. *Mol Plant Pathol* **11**: 83-92.

Tyler BM. 2001. Genetics and genomics of the oomycete-host interface. *Trends Genet* **17**: 611-614.

Tyler BM. 2017. The fog of war: how network buffering protects plants' defense secrets from pathogens. *PLoS Genet* **13**: e1006713.

Varbanova M, Porter K, Lu F, Ralph J, Hammerschmidt R, Jones AD, Day B. 2011. Molecular and biochemical basis for stress-induced accumulation of free and bound p-coumaraldehyde in cucumber. *Plant Physiol* **157**: 1056-1066.

Vega-Arreguin JC, Jalloh A, Bos JI, Moffett P. 2014. Recognition of an Avr3a homologue plays a major role in mediating nonhost resistance to *Phytophthora capsici* in *Nicotiana* species. *Mol Plant Microbe Interact* **27**: 770-780.

Wallace IM, O'Sullivan O, Higgins DG, Notredame C. 2006. M-Coffee: combining multiple sequence alignment methods with T-Coffee. *Nucleic Acids Res* **34**: 1692-1699.

Wang QQ, Han CZ, Ferreira AO, Yu XL, Ye WW, Tripathy S, Kale SD, Gu BA, Sheng YT, Sui YY, et al. 2011. Transcriptional programming and functional interactions within the *Phytophthora sojae* RXLR effector repertoire. *Plant Cell* **23**: 2064-2086.

Wang X, Boevink P, McLellan H, Armstrong M, Bukharova T, Qin Z, Birch PR. 2015. A host KH RNA-binding protein is a susceptibility factor targeted by an RXLR effector to promote late blight disease. *Mol Plant* **8**: 1385-1395.

Wang Y, Wang Y. 2018. Trick or treat: microbial pathogens evolved apoplastic effectors modulating plant susceptibility to infection. *Mol Plant Microbe Interact* **31**: 6-12.

Wang Y, Xu Y, Sun Y, Wang H, Qi J, Wan B, Ye W, Lin Y, Shao Y, Dong S, et al. 2018. Leucine-rich repeat receptor-like gene screen reveals that Nicotiana RXEG1 regulates glycoside hydrolase 12 MAMP detection. *Nat Commun* **9**: 594.

Win J, Krasileva KV, Kamoun S, Shirasu K, Staskawicz BJ, Banfield MJ. 2012. Sequence divergent RXLR effectors share a structural fold conserved across plant pathogenic oomycete species. *PLoS Pathog* **8**: e1002400.

Yaeno T, Li H, Chaparro-Garcia A, Schornack S, Koshiba S, Watanabe S, Kigawa T, Kamoun S, Shirasu K. 2011. Phosphatidylinositol monophosphate-binding interface in the oomycete RXLR effector AVR3a is required for its stability in host cells to modulate plant immunity. *Proc Natl Acad Sci USA* **108**: 14682-14687.

Yoo SD, Cho YH, Sheen J. 2007. *Arabidopsis* mesophyll protoplasts: a versatile cell system for transient gene expression analysis. *Nat Protoc* **2**: 1565-1572.

Youn B, Camacho R, Moinuddin SG, Lee C, Davin LB, Lewis NG, Kang C. 2006. Crystal structures and catalytic mechanism of the *Arabidopsis* cinnamyl alcohol dehydrogenases AtCAD5 and AtCAD4. *Org Biomol Chem* **4**: 1687-1697.

Zhang X, Henriques R, Lin SS, Niu QW, Chua NH. 2006. *Agrobacterium*-mediated transformation of *Arabidopsis thaliana* using the floral dip method. *Nat Protoc* **1**: 641-646.

Zheng Z, Qamar SA, Chen Z, Mengiste T. 2006. Arabidopsis WRKY33 transcription factor is required for resistance to necrotrophic fungal pathogens. *Plant J* **48**: 592-605.

Figures Legends

Fig 1. Avr3a-like effectors are distributed widely across *Phytophthora* species.

(**a**) The number of Avr3a-like (Avr3aL) sequence matches in the genome of 10 surveyed *Phytophthora* species. The phylogeny is based on previous description of *Phytophthora* genus (Kroon *et al.*, 2012). (**b**) Phylogenetic analysis of Avr3a-like effectors in the genus of *Phytophthora*. The Avr3a-like effectors that specifically expanded in *P. capsici* were highlighted in yellow. The six query sequences were indicated by black triangles, and the PcAvr3a-like effectors further characterized in this study were indicated by red circles. The phylogenetic relationship was inferred by PhyML based on alignment generated with M-Coffee. Color key (from green to red) indicates the aLRT SH-like branch support value, from low to high. Black dot marks the root of phylogenetic tree.

Fig 2. Multiple *Phytophthora* Avr3a-like effectors interact with CAD7.

(**a**) *A. thaliana* CAD7 (AtCAD7) interacts with Avr3a-like effectors as determined by a Y2H assay. AtCAD7$_{85\text{-}358}$ on pGADT7 (AD) vector, which was derived from cDNA library screening, was used to confirm the interactions with effectors (PsAvr1b, PiAvr3a^{KI}, PiAvr3a^{EM}, PcAvr3a1, PcAvr3a12, and PITG_23129) cloned into pGBKT7 (BD). Yeast transformants were separately transferred onto SD/-Leu/-Trp (SD-LT), SD-Leu/-Trp/-His/-Ade (SD-LTHA), and SD/-Leu/-Trp/-His/-Ade medium with 40 µg/ml X-α-gal (SD-LTHA/X). The growth of yeast transformants on SD-LT medium demonstrated successful transformations. The growth of yeast transformants on SD-LTHA (*His* and *Ade* reporter genes activated) and blue color on SD-LTHA/X (*LacZ* reporter gene activated) indicate interactions. Pictures were taken after 3 days of culture. (**b**) AtCAD7 interacts with Avr3a-like effectors in the BiFC assay. The effectors fused with the N terminus of YFP and AtCAD7 fused with the C terminus of YFP were transiently co-expressed in *N. benthamiana* and examined by confocal microscopy at 3 days post infiltration (dpi). The complementation of fluorescence indicates interaction between assayed proteins. The candidate RXLR effector PITG_23129 from *P. infestans* served as a control.

Fig 3. Host CAD7s are conserved targets of *Phytophthora* Avr3a-like effectors.

(**a-c**) AtCAD7 interacts with Avr3a-like effectors from *P. capsici* in BiFC (**a**), Y2H (**b**) and Co-IP (**c**) assays. The proteins used for Co-IP were derived from *N. benthamiana* co-expressed AtCAD7-Myc with GFP-PcAvr3a1, GFP-PcAvr3a3, GFP-PcAvr3a11, GFP-PcAvr3a6, GFP-PcAvr3a12, GFP-PcAvr3a5, GFP-PcAvr3a14, and GFP-PITG_23129. Total proteins were then subjected to incubation with GFP-Trap_A beads and anti-Myc (α-Myc) immune blotting of the output was used to identify the co-immunoprecipitation of AtCAD7-Myc with GFP-effectors. (**d-f**) *N. benthamiana* CAD7 (NbCAD7) interacts with Avr3a-like effectors from *P. capsici* in BiFC (**d**), Y2H **(e)** and Co-IP (**f**) assays. In Co-IP assays, NbCAD7-FLAG was coexpressed with GFP-PcAvr3a1, GFP-PcAvr3a12, GFP-PcAvr3a128, and GFP-PITG_23129. Anti-FLAG (α-FLAG) immune blotting of the output was used to identify the co-immunoprecipitation of NbCAD7-FLAG with GFP-effectors. (**g-i**) NbCAD7 interacts with Avr3a-like effectors from *P. infestans* in BiFC (**g**), Co-IP (**h**), and Y2H (**i**) assays. In Co-IP assays, NbCAD7-Myc was coexpressed with GFP-PiAvr3a^{EM}, GFP-PiAvr3a^{KI}, and GFP-PcAvr3a1. Anti-Myc immune blotting of the output was used to identify the co-immunoprecipitation of NbCAD7-Myc with GFP-effectors. The complete proteins of GFP-effectors were marked with red asterisks. Note that all these Co-IP assays are qualitative rather than quantitative experiments.

Fig 4. Silencing of *CAD7* enhances resistance against *Phytophthora*.

(**a-c**) Silencing of *AtCAD7* decreased the colonization of *P. capsici* in *Arabidopsis*. (**a**) *AtCAD7* is down-regulated in two independent RNAi lines (Ri.1 and Ri.2) compared with that of the wild type Col-0 (WT). Total RNA extracted from Ri.1, Ri.2, and the WT plants was used for quantification of *AtCAD7* transcripts by qRT-PCR. Constitutively expressed *AtUBC9* was used as a reference gene. Error bars represent the standard deviations from three individual transgenic plants derived from each independent transformation line. (**b**) Trypan blue staining showed that the colonization of *P. capsici* in Ri.1 and Ri.2 leaves was decreased as compared to that in WT. (**c**) Statistical analyses of the lesion diameters of *P. capsici* infection in the WT and RNAi plants at 2 days post inoculation (dpi). (**d-h**) Silencing of *NbCAD7* decreased the colonization of *P. capsici* and *P. infestans* in *N. benthamiana*. (**d**) Statistical analyses of qRT-PCR results showed that *NbCAD7* was down-regulated by 50% to

82% in TRV::*NbCAD7* (*tNb7*) plants as compared to the TRV::*GFP* (*tGFP*) plants. Total RNA extracted from *N. benthamiana* expressing TRV::*NbCAD7* and TRV::*GFP* at 4 weeks after infiltration was used for qRT-PCR. Constitutively expressed *NbEF1α* was used as a reference gene. Three biological replicates were independently derived from VIGS plants and each replicate contained six leaves from three VIGS plants (two leaves from each plant) in the same batch. Error bars represent the standard deviations from three individual VIGS plants. Trypan blue staining showed that the lesions caused by *P. capsici* (**e**) and *P. infestans* (**f**) that developed in *N. benthamiana* leaves expressing TRV::*NbCAD7* were smaller than that in the control leaves expressing TRV::*GFP*. The inoculations were performed 4 weeks after agro-infiltration with TRV constructs. *P. capsici* infections were observed at 2 dpi and *P. infestans* infections were observed at 8 dpi. Boxplots showing the statistical analyses of lesion diameters in *tNb7* and *tGFP* leaves infected by *P. capsici* (**g**) and *P. infestans* (**h**). Each boxplot illustrates lesion diameters measured from more than 10 leaves from the same batch; each inoculation test was repeated at least four times with similar results. In (**c**, **g**, **h**), the upper quartile, median, and lower quartile were showed in each box, while the bars outside the box indicated the 5th and 95th percentiles. In (**a**, **c**, **d**, **g**, **h**), one-sided *t*-tests were used to assess significances, "*" indicates *P*-value < 0.05, and "***" indicates *P*-value < 0.001.

Fig 5. Overexpression of *AtCAD7* decreases resistance against *P. capsici*.

(**a**) *AtCAD7* is up-regulated in two independent overexpression lines (OE7) compared with wild-type Col-0 (WT) in the absence of infection. Constitutively expressed *AtUBC9* was used as a reference gene. Error bars represent the standard deviations from three individual transgenic plants derived from each independent transformation line. (**b**) Trypan blue staining showed that colonization by *P. capsici* increased in OE7 as compared to WT. (**c**) Statistical analyses of the lesion diameters of *P. capsici* infection in the WT and OE7 plants at 2 dpi. Each boxplot illustrates the lesion diameters measured from at least 10 leaves. The experiment was repeated at least four times with similar results. (**d**) Statistical analyses of the *P. capsici* biomass in the infected leaves of the WT and OE7 plants. The biomass was measured as the ratio of the pathogen DNA relative to the host plant DNA as determined by qRT-PCR. *P. capsici ACTIN* (*PcACTIN*) and *Arabidopsis UBC9* (*AtUBC9*) were used as reference genes in qPCR analyses. The biomass in the WT plants was set to 1. Each boxplot summarizes the biomass measured from six individuals. The leaves of 4-week old *Arabidopsis* were inoculated with zoospores of *P. capsici* strain LT263. In (**c**, **d**), the upper quartile, median, and lower quartile were showed in each box, while the bars outside the box indicated the 5th and 95th percentiles. In (**a**, **c**, **d**), one-sided *t*-tests were used to assess significances, "**" indicates *P*-value < 0.01 and "***" indicates *P*-value < 0.001.

Fig 6. Mutations in the predicted enzyme activity sites of AtCAD7 do not affect its function as a negative regulator of plant immunity or its interaction with Avr3a-like effectors.

(**a**) Overview of two AtCAD7 mutants (AtCAD7m1 and AtCAD7m2) that were mutated at the enzyme activity sites. (**b-c**) Both AtCAD7m1 and AtCAD7m2 interacted with Avr3a-like effectors in the BiFC assay. PITG_23129 was used as a control. (**d**) AtCAD7m2 interacted with Avr3a-like effectors in Co-IP assays. The proteins used for Co-IP were derived from *N. benthamiana* co-expressing AtCAD7m2-Myc with GFP-PcAvr3a14, GFP-PcAvr3a5, GFP-PcAvr3a12, and GFP-PITG_23129. Total proteins were then subjected to incubation with GFP-Trap_A beads and anti-Myc (*α*-Myc) immune blotting of the output was used to identify the co-immunoprecipitation of AtCAD7-Myc with GFP-effectors. The complete proteins of GFP-effectors are marked with red asterisks. (**e**) *AtCAD7* is up-regulated in OE7m1 and OE7m2 plants compared with that of the wild type Col-0 (WT). Total RNA extracted from OE7m1.1, OE7m1.2, OE7m2.1, OE7m2.2, and the WT plants was used for quantification of *AtCAD7* transcripts by qRT-PCR. Constitutively expressed *AtUBC9* was used as a reference gene. Error bars represent the standard deviations from three individual transgenic plants of each independent transformation line. (**f**) Trypan blue staining showed that the colonization of *P. capsici* in OE7m1 and OE7m2 leaves increased compared with that in the WT. (**g**) Statistical analysis indicates that the lesion diameters in OE7m1 and OE7m2 leaves were significantly larger than in the WT. OE7m1 and OE7m2 represent the transgenic *Arabidopsis* lines expressing AtCAD7 mutants. All leaves were challenged with zoospores of *P. capsici* LT263 and the phenotypes were observed at 2 dpi. The experiments were repeated three times with similar results. (**h**) Statistical analyses of the *P. capsici* biomass in the infected leaves of the WT (Col-0) and OE7m plants. The biomass was measured as the ratio of the pathogen DNA relative to the host plant DNA as determined by qRT-PCR. *P. capsici* ACTIN (*PcACTIN*) and *Arabidopsis UBC9* (*AtUBC9*) were used as reference genes in qRT-PCR analysis. Biomass of the WT plants was set to 1. Each boxplot summarizes the biomass measured from six individuals. In (**g**, **h**), the upper quartile, median, and lower quartile were showed in each box, while the bars outside the box indicated the 5th and 95th percentiles. In (**e**, **g**, **h**), one-sided *t*-tests were used to assess significances, "*" indicates *P*-value < 0.05, "**" indicates *P*-value < 0.01 and "***" indicates *P*-value < 0.001.

Fig 7. ***CAD7*** **suppresses PTI in the host plant.**

(**a**) Three different levels of plant cell death are defined according to the percentage of the cell death area developed in the infiltration area. (**b-c**) Phenotypes (**b**) and statistical analyses (**c**) of plant cell death triggered by INF1 in *N. benthamiana* expressing TRV::*NbCAD7* (*tNb7*) and TRV::*GFP* (*tGFP*) indicate that silencing of *NbCAD7* promotes ICD specifically. (**d-e**) Phenotypes (**d**) and statistical analyses (**e**) of the plant cell death triggered by INF1 in *N. benthamiana* overexpressing *NbCAD7* and *GFP* indicate that overexpression of *NbCAD7* attenuates ICD. In (**c**) and (**e**), the cell death was observed from their first appearance; statistical analyses were based on the most representative stage of the cell death as indicated in the bottom of each column. The differences in cell death in the *N. benthamiana* leaves were assessed by one-sided Wilcoxon rank-sum tests. Numbers above the columns indicate the total number of infiltration sites used for statistical analyses. (**f**) Silencing of *NbCAD7* attenuates the ability of *PiAvr3a* to suppress ICD. The ability of *PiAvr3a* to suppress ICD is compromised in *tNb7* plants as compared to control *tGFP* plants. Percentages indicate the inhibition efficiency of *PiAvr3a*^{KI} to suppress ICD in *tNb7* plants and *tGFP* plants at three days post infiltration. The differences of cell death percentage in *N. benthamiana* leaves were assessed using a Fisher’s exact test. Each experiment was repeated at least three times with highly similar results. (**g**) Aniline blue and DAB staining assays to show callose deposition and ROS burst, respectively. *Arabidopsis* leaves from *AtCAD7*-overexpression lines (OE7), *AtCAD7*-silencing lines (Ri) and the wild-type Col-0 (WT) were treated with 1 μM flg22 before staining. (**h**) Violin plot showing the relative intensity of callose deposition from multiple leaves of *Arabidopsis*. (**i**) Violin plot showing the relative intensity of ROS burst from multiple leaves of *Arabidopsis*. In (**h-i**), the intensities were quantified by the number of callose or ROS-corresponding pixels and were normalized with the intensities in WT, and one-sided *t*-tests were used to assess significances. In (**c**, **e**, **f**, **h**, and **i)**, “*” indicates *P*-value < 0.05, “**” indicates *P*-value < 0.01, “***” indicates *P*-value < 0.001, and “****” indicates *P*-value < 0.0001.

Fig 8. AtCAD7 is stabilized by Avr3a-like effectors in a 26S proteasome-dependent manner.

Proteins were derived from *N. benthamiana* plants co-expressing *AtCAD7-Myc* and *GFP-PiAvr3a*^{KI}, *GFP-PiAvr3a*^{EM}, *GFP-PcAvr3a12*, or the control (*GFP*) at two days post *Agrobacterium* infiltration. Proteasome inhibitor MG132 or control dimethyl sulfoxide (DMSO, i.e. -MG132) was infiltrated 12 hours before harvest. Total proteins were extracted and subjected to SDS-PAGE, followed by anti-Myc (α-Myc) immuno-detection of AtCAD7-Myc in the absence or presence of MG132. The recombinant fusion proteins of GFP-effectors are marked with red asterisks. Protein loading is shown by Ponceau S staining. RT-PCR assays for *AtCAD7* expression in *N. benthamiana* were performed to assure equal levels of RNA transcripts. *NbEF1α* was used an internal control.

Fig 9. Proposed model for the role of CAD7 in the negative regulation of plant immunity.

Multiple Avr3a-like effectors target and stabilize CAD7, which suppresses PTI as indicated by the suppression of INF1-triggered cell death, callose deposition, ROS burst, and *WRKY33* transcription. The PTI suppression renders plants susceptible to pathogen infection. During evolution, CAD7 diversification was driven by interactions with *Phytophthora* pathogens, being frequently exploited as a susceptibility factor targeted by pathogen effectors. Colored circle dots represent multiple Avr3a-like effectors.

Supporting Information

Fig S1. Arrangement of PcAvr3a-like genes in the LT263 genome.

Fig S2. Transcript levels of PcAvr3a-like effect genes during infection of *Arabidopsis thaliana* and *Nicotiana benthamiana*.

Fig S3. Residues conserved among Avr3a-like effectors used in this study.

Fig S4. Immuno-detection of proteins from *N. benthamiana* expressing BiFC constructs.

Fig S5. Phylogenetic analysis of the plant CAD family proteins.

Fig S6. *AtCAD7, AtCAD6* and *AtCAD8* are induced during *P. capsici* infection.

Fig S7. Interaction of AtCAD6 and AtCAD8 with Avr3a-like effectors.

Fig S8. Co-localization analysis of CAD7 and effectors.

Fig S9. Expression of *CAD* genes in *CAD7*-silenced plants.

Fig S10. Morphology of *AtCAD7*-silenced *Arabidopsis* plants (Ri) (a), virus induced *NbCAD7* silenced *N. benthamiana* plants TRV::*NbCAD7* (tNb7) (b), and transgenic *AtCAD7* (OE7) or *AtCAD7m* (OE7m) *Arabidopsis* plants (c).

Fig S11. Over-expression of *NbCAD7* does not promote *P. capsici* infection.

Fig S12. Amino acid sequence alignment of AtCAD7, AtCAD5, and PtSAD.

Fig S13. Histochemical analysis of lignified tissues of *AtCAD7* silenced plants (Ri), *AtCAD7* overexpression plants OE7 and *AtCAD7m* transgenic plants OE7m.

Fig S14. Wild-type and mutant AtCAD7 proteins could suppress INF1-triggered cell death.

Fig S15. The expression of defense-related genes in *AtCAD7*-overexpressing *Arabidopsis* plants.

Fig S16. AtCAD7 is stabilized by Avr3a-like effectors in *Arabidopsis* protoplasts.

Fig S17. NbCMPG1 proteins are not bound by NbCAD7 nor by PcAvr3a12.

Table S1. Primers used in this study.

Dataset S1. The Avr3a-like sequences identified in this study.

Dataset S2. The CAD homologs identified in this study.

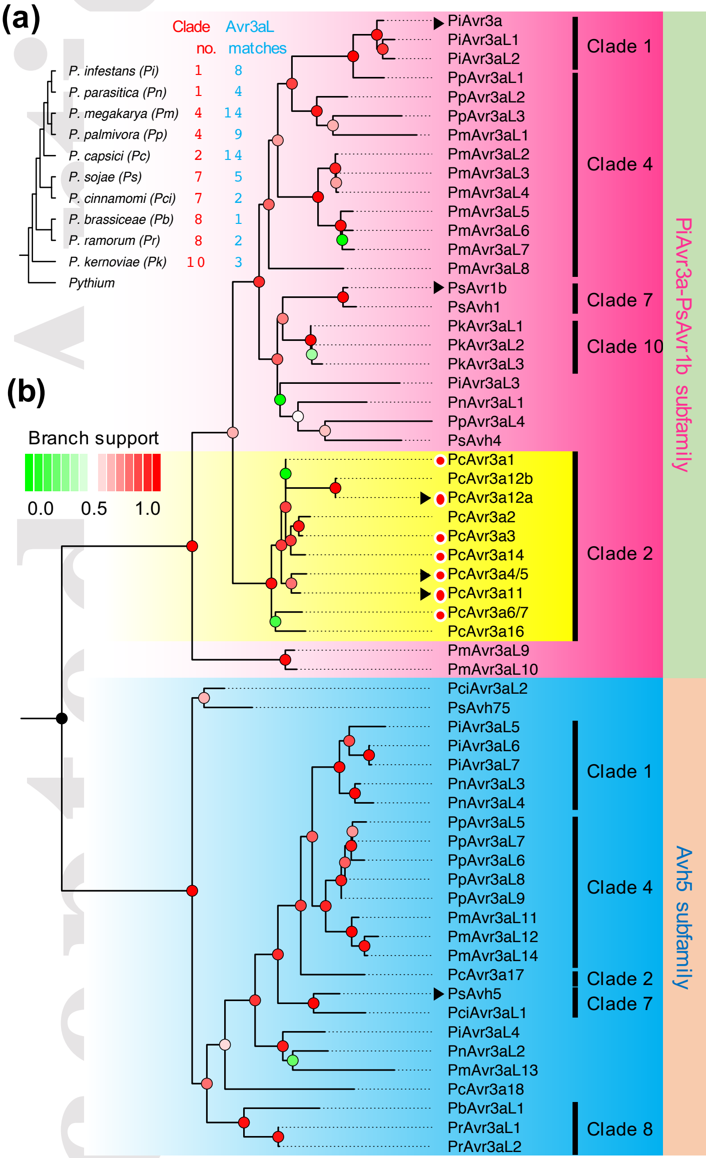
(a)
Clade no.
Avr3aL matches
P. infestans (Pi) 1 8
P. parasitica (Pn) 1 4
P. megakarya (Pm) 4 14
P. palmivora (Pp) 4 9
P. capsici (Pc) 2 14
P. sojae (Ps) 7 5
P. cinnamomi (Pci) 7 2
P. brassiceae (Pb) 8 1
P. ramorum (Pr) 8 2
P. kernoviae (Pk) 10 3
Pythium
(b)
Branch support
0.0
0.5
1.0
PiAvr3a
PiAvr3aL1
PiAvr3aL2
PpAvr3aL1
PpAvr3aL2
PpAvr3aL3
PmAvr3aL1
PmAvr3aL2
PmAvr3aL3
PmAvr3aL4
PmAvr3aL5
PmAvr3aL6
PmAvr3aL7
PmAvr3aL8
PsAvr1b
PsAvh1
PkAvr3aL1
PkAvr3aL2
PkAvr3aL3
PiAvr3aL3
PnAvr3aL1
PpAvr3aL4
PsAvh4
PcAvr3a1
PcAvr3a12b
PcAvr3a12a
PcAvr3a2
PcAvr3a3
PcAvr3a14
PcAvr3a4/5
PcAvr3a11
PcAvr3a6/7
PcAvr3a16
PmAvr3aL9
PmAvr3aL10
PciAvr3aL2
PsAvh75
PiAvr3aL5
PiAvr3aL6
PiAvr3aL7
PnAvr3aL3
PnAvr3aL4
PpAvr3aL5
PpAvr3aL7
PpAvr3aL6
PpAvr3aL8
PpAvr3aL9
PmAvr3aL11
PmAvr3aL12
PmAvr3aL14
PcAvr3a17
PsAvh5
PciAvr3aL1
PiAvr3aL4
PnAvr3aL2
PmAvr3aL13
PcAvr3a18
PbAvr3aL1
PrAvr3aL1
PrAvr3aL2
Clade 1
Clade 4
Clade 7
Clade 10
Clade 2
Clade 1
Clade 4
Clade 2
Clade 7
Clade 8
PiAvr3a-PsAvr1b subfamily
Avh5 subfamily

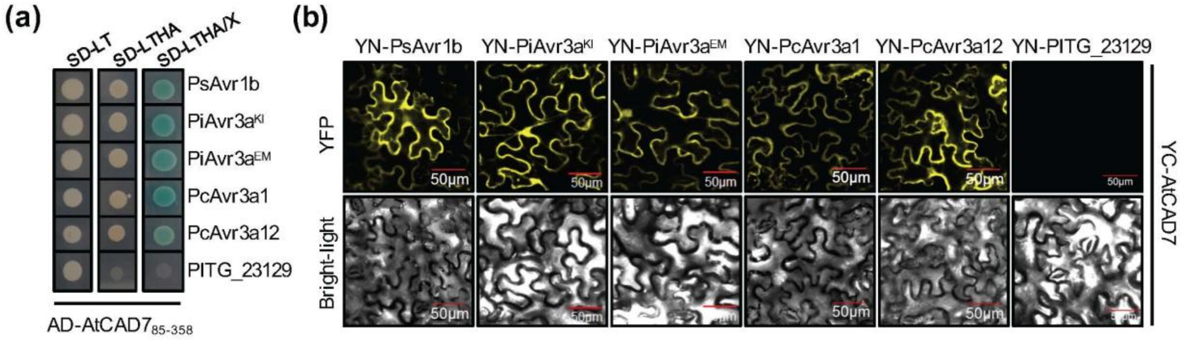
(a)
SD-LT
SD-LTHA
SD-LTHA/X
PsAvr1b
PiAvr3aKI
PiAvr3aEM
PcAvr3a1
PcAvr3a12
PITG_23129
AD-AtCAD785-358
(b)
YN-PsAvr1b
YN-PiAvr3aKI
YN-PiAvr3aEM
YN-PcAvr3a1
YN-PcAvr3a12
YN-PITG_23129
YFP
Bright-light
YC-AtCAD7
50μm

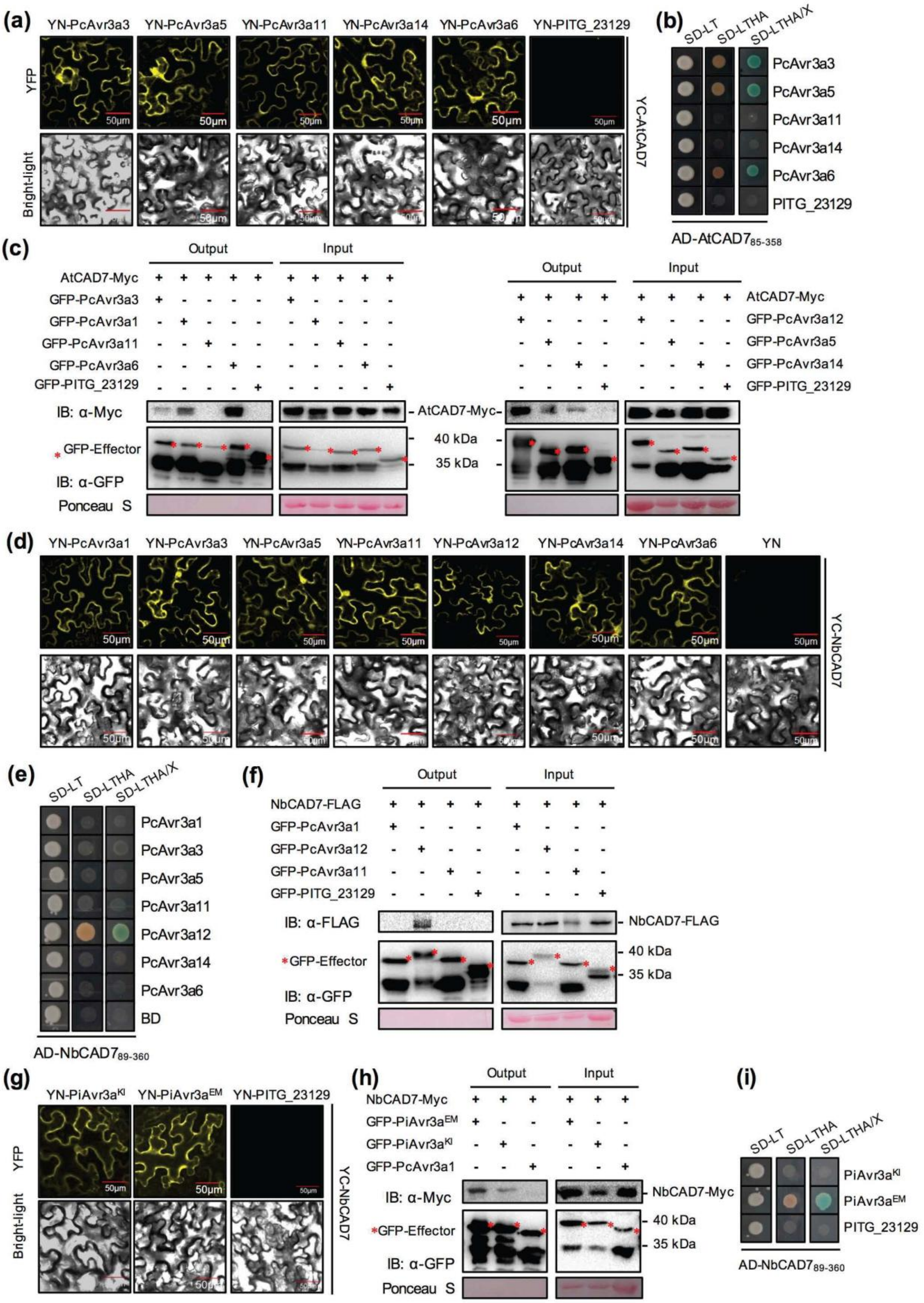
(a)
YN-PcAvr3a3
YN-PcAvr3a5
YN-PcAvr3a11
YN-PcAvr3a14
YN-PcAvr3a6
YN-PITG_23129
YFP
Bright-light
YC-AtCAD7
50μm
(b)
SD-LT
SD-LTHA
SD-LTHA/X
PcAvr3a3
PcAvr3a5
PcAvr3a11
PcAvr3a14
PcAvr3a6
PITG_23129
AD-AtCAD7$_{85-358}$
(c)
Output
Input
AtCAD7-Myc
GFP-PcAvr3a3
GFP-PcAvr3a1
GFP-PcAvr3a11
GFP-PcAvr3a6
GFP-PITG_23129
GFP-PcAvr3a12
GFP-PcAvr3a5
GFP-PcAvr3a14
IB: α-Myc
AtCAD7-Myc
*GFP-Effector
IB: α-GFP
Ponceau S
40 kDa
35 kDa
(d)
YN-PcAvr3a1
YN-PcAvr3a3
YN-PcAvr3a5
YN-PcAvr3a11
YN-PcAvr3a12
YN-PcAvr3a14
YN-PcAvr3a6
YN
YC-NbCAD7
50μm
(e)
SD-LT
SD-LTHA
SD-LTHA/X
PcAvr3a1
PcAvr3a3
PcAvr3a5
PcAvr3a11
PcAvr3a12
PcAvr3a14
PcAvr3a6
BD
AD-NbCAD7$_{89-360}$
(f)
Output
Input
NbCAD7-FLAG
GFP-PcAvr3a1
GFP-PcAvr3a12
GFP-PcAvr3a11
GFP-PITG_23129
IB: α-FLAG
NbCAD7-FLAG
*GFP-Effector
IB: α-GFP
Ponceau S
40 kDa
35 kDa
(g)
YN-PiAvr3a^{KI}
YN-PiAvr3a^{EM}
YN-PITG_23129
YFP
Bright-light
YC-NbCAD7
50μm
(h)
Output
Input
NbCAD7-Myc
GFP-PiAvr3a^{EM}
GFP-PiAvr3a^{KI}
GFP-PcAvr3a1
IB: α-Myc
NbCAD7-Myc
*GFP-Effector
IB: α-GFP
Ponceau S
40 kDa
35 kDa
(i)
SD-LT
SD-LTHA
SD-LTHA/X
PiAvr3a^{KI}
PiAvr3a^{EM}
PITG_23129
AD-NbCAD7$_{89-360}$

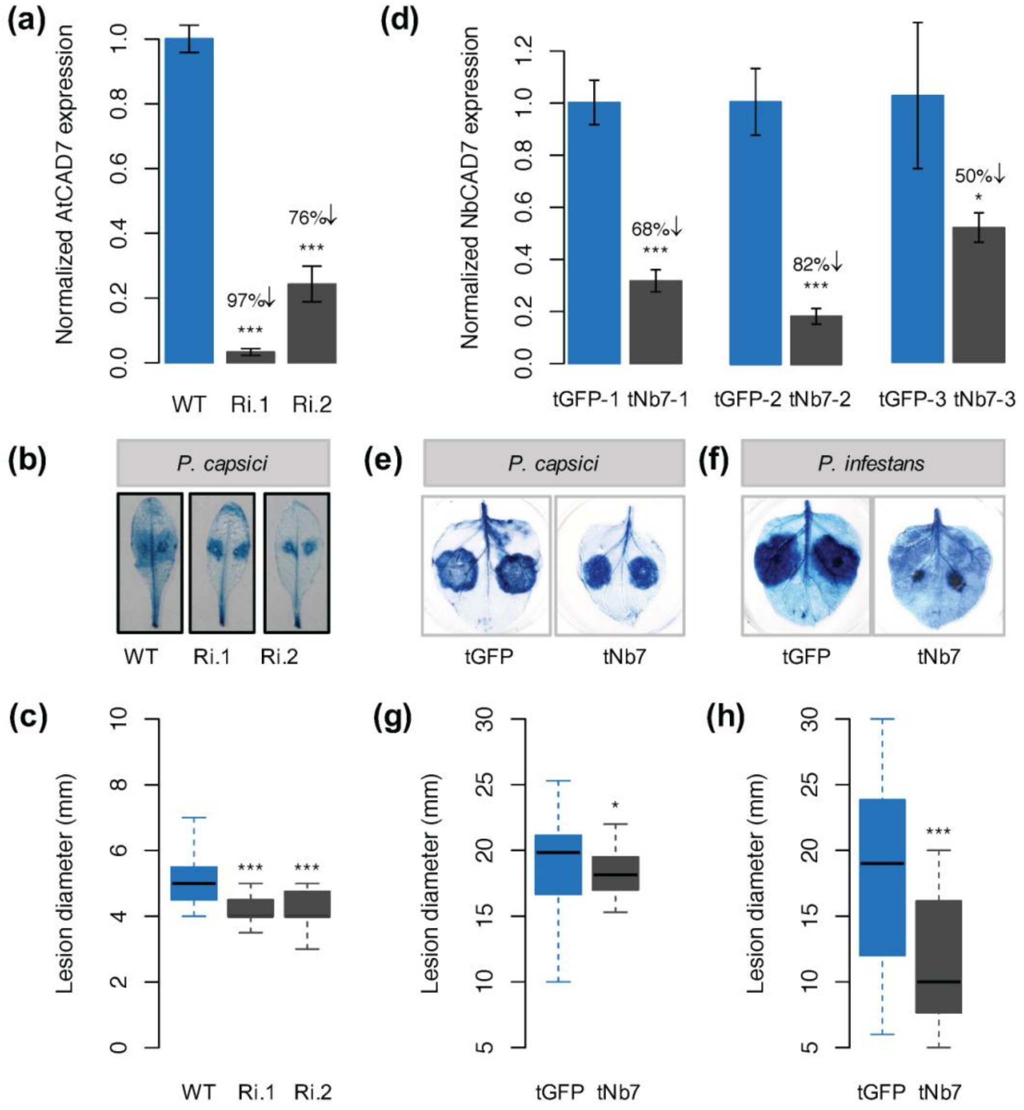
(a)
Normalized AtCAD7 expression
0.0
0.2
0.4
0.6
0.8
1.0
97%↓
***
76%↓
***
WT
Ri.1
Ri.2
(d)
Normalized NbCAD7 expression
0.0
0.2
0.4
0.6
0.8
1.0
1.2
68%↓
***
82%↓
***
50%↓
*
tGFP-1
tNb7-1
tGFP-2
tNb7-2
tGFP-3
tNb7-3
(b)
P. capsici
WT
Ri.1
Ri.2
(e)
P. capsici
tGFP
tNb7
(f)
P. infestans
tGFP
tNb7
(c)
Lesion diameter (mm)
0
2
4
6
8
10
***
***
WT
Ri.1
Ri.2
(g)
Lesion diameter (mm)
5
10
15
20
25
30
*
tGFP
tNb7
(h)
Lesion diameter (mm)
5
10
15
20
25
30
***
tGFP
tNb7

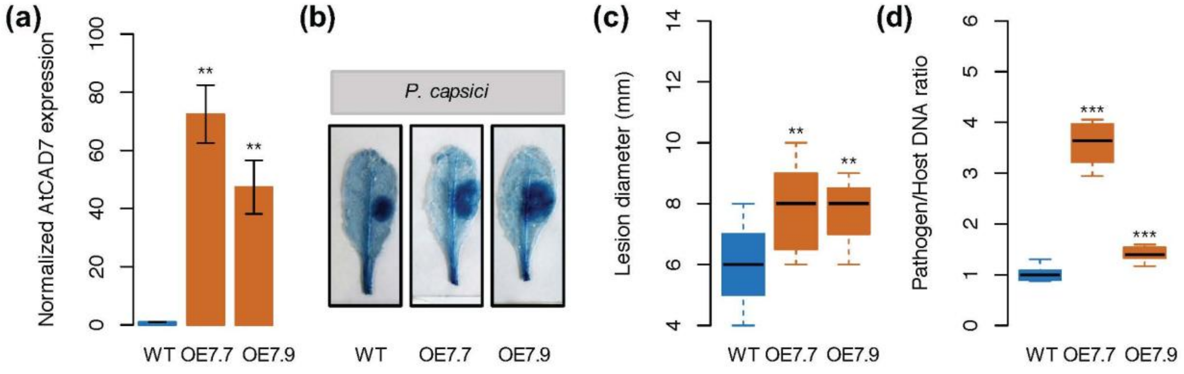
(a)
Normalized AtCAD7 expression
0
20
40
60
80
100
**
**
WT OE7.7 OE7.9
(b)
P. capsici
WT
OE7.7
OE7.9
(c)
Lesion diameter (mm)
4
6
8
10
12
14
**
**
WT OE7.7 OE7.9
(d)
Pathogen/Host DNA ratio
0
1
2
3
4
5
6
***
***
WT OE7.7 OE7.9

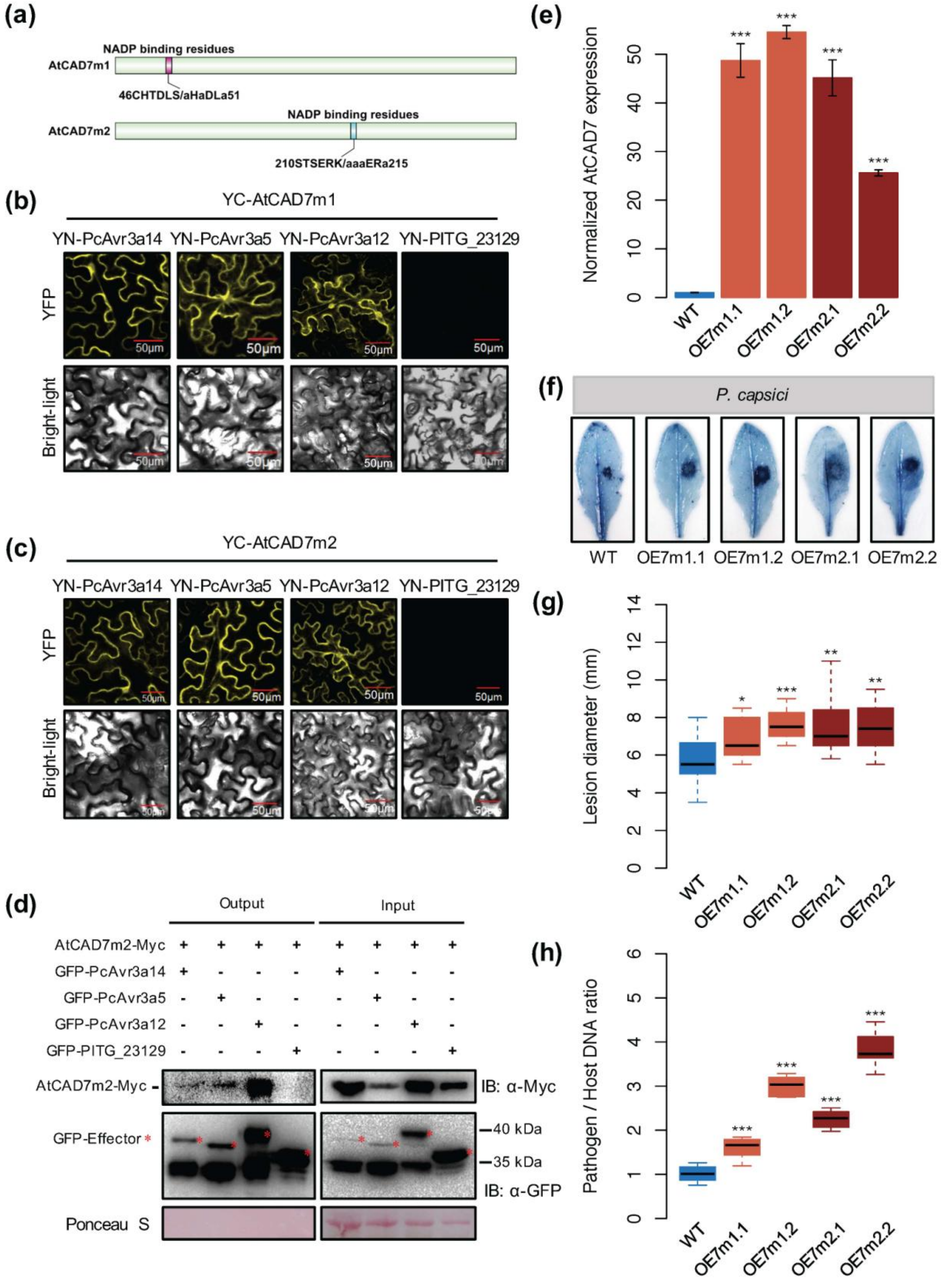
(a)
NADP binding residues
AtCAD7m1
46CHTDLS/aHaDLa51
NADP binding residues
AtCAD7m2
210STSERK/aaaERa215
(b)
YC-AtCAD7m1
YN-PcAvr3a14
YN-PcAvr3a5
YN-PcAvr3a12
YN-PITG_23129
YFP
Bright-light
50μm
(c)
YC-AtCAD7m2
YN-PcAvr3a14
YN-PcAvr3a5
YN-PcAvr3a12
YN-PITG_23129
YFP
Bright-light
50μm
(d)
Output
Input
AtCAD7m2-Myc
GFP-PcAvr3a14
GFP-PcAvr3a5
GFP-PcAvr3a12
GFP-PITG_23129
AtCAD7m2-Myc
IB: α-Myc
GFP-Effector *
40 kDa
35 kDa
IB: α-GFP
Ponceau S
(e)
Normalized AtCAD7 expression
0
10
20
30
40
50
***
WT
OE7m1.1
OE7m1.2
OE7m2.1
OE7m2.2
(f)
P. capsici
WT
OE7m1.1
OE7m1.2
OE7m2.1
OE7m2.2
(g)
Lesion diameter (mm)
0
2
4
6
8
10
12
14
*
***
**
WT
OE7m1.1
OE7m1.2
OE7m2.1
OE7m2.2
(h)
Pathogen / Host DNA ratio
0
1
2
3
4
5
6
***
WT
OE7m1.1
OE7m1.2
OE7m2.1
OE7m2.2

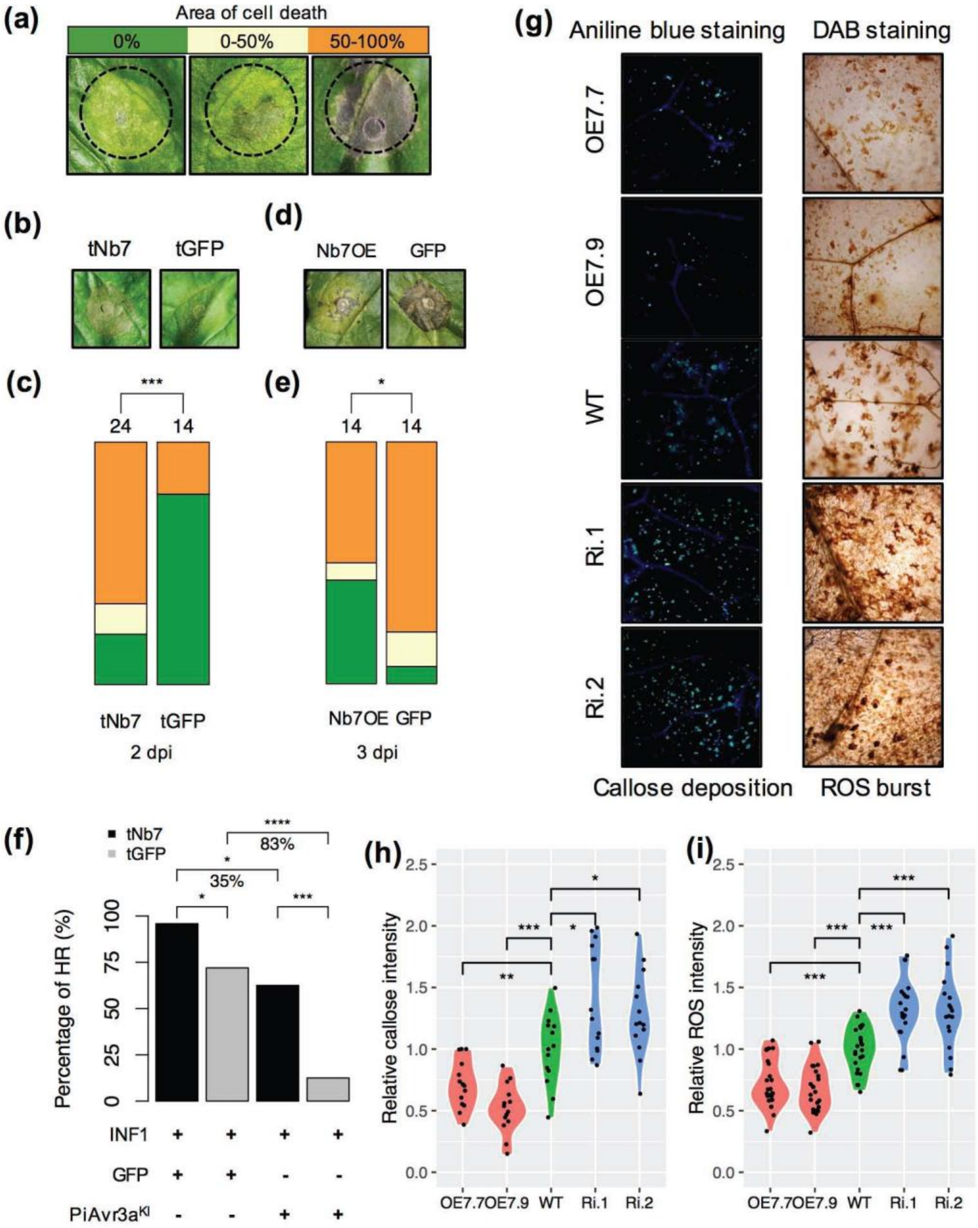
(a)
Area of cell death
0%
0-50%
50-100%
(b)
tNb7
tGFP
(d)
Nb7OE
GFP
(c)
***
24
14
tNb7
tGFP
2 dpi
(e)
*
14
14
Nb7OE GFP
3 dpi
(g)
Aniline blue staining
DAB staining
OE7.7
OE7.9
WT
Ri.1
Ri.2
Callose deposition
ROS burst
(f)
■ tNb7
■ tGFP
****
83%
*
35%
*
***
Percentage of HR (%)
0
25
50
75
100
INF1 + + + +
GFP + + - -
PiAvr3a^{KI} - - + +
(h)
Relative callose intensity
0.0
0.5
1.0
1.5
2.0
2.5
*
***
*
**
OE7.7
OE7.9
WT
Ri.1
Ri.2
(i)
Relative ROS intensity
0.0
0.5
1.0
1.5
2.0
2.5
***
***
***
***
OE7.7
OE7.9
WT
Ri.1
Ri.2

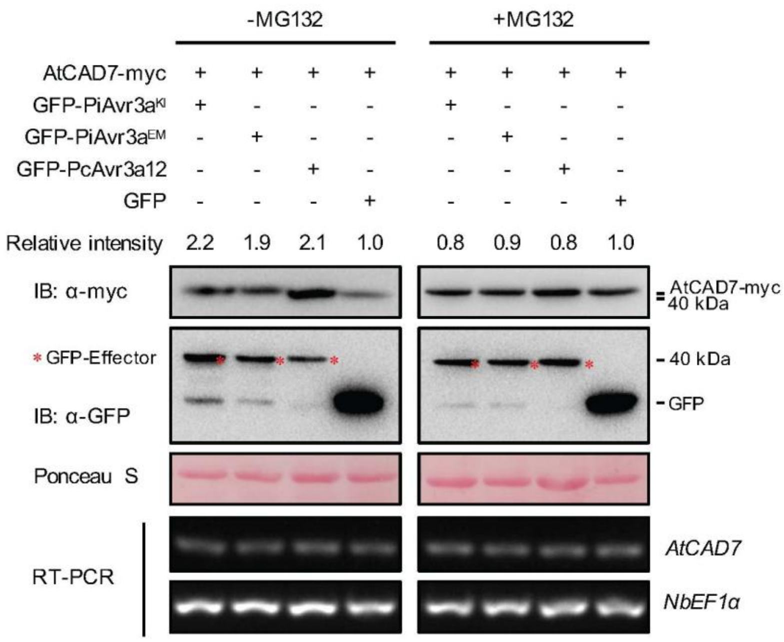
-MG132
+MG132
AtCAD7-myc
GFP-PiAvr3aKI
GFP-PiAvr3aEM
GFP-PcAvr3a12
GFP
Relative intensity
2.2
1.9
2.1
1.0
0.8
0.9
0.8
1.0
IB: α-myc
AtCAD7-myc
40 kDa
* GFP-Effector
IB: α-GFP
40 kDa
GFP
Ponceau S
RT-PCR
AtCAD7
NbEF1α

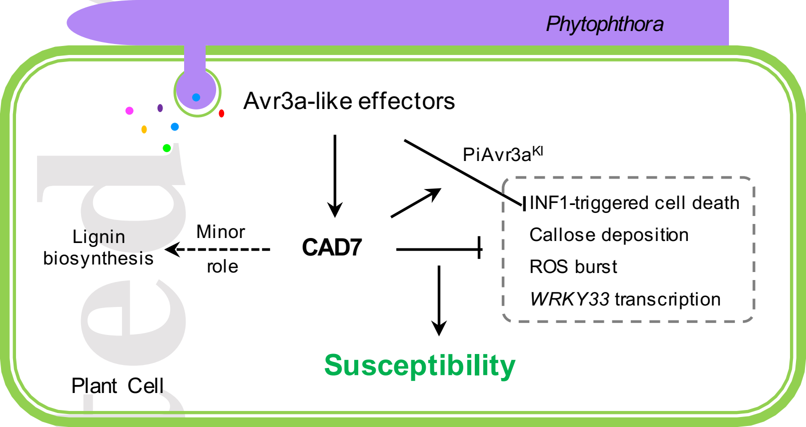
Phytophthora
Avr3a-like effectors
PiAvr3a^{KI}
INF1-triggered cell death
Callose deposition
ROS burst
WRKY33 transcription
Lignin biosynthesis
Minor role
CAD7
Susceptibility
Plant Cell